



TRIBHUVAN UNIVERSITY
INSTITUTE OF ENGINEERING
PULCHOWK CAMPUS

Thesis No: M-73-MSMDE-2021-2023

**Development and Experimental Verification of Manual Piston Driven Hypersonic
Shock Tunnel**

by

Akin Chhetri

A THESIS

**SUBMITTED TO THE DEPARTMENT OF MECHANICAL AND AEROSPACE
ENGINEERING IN PARTIAL FULFILLMENT OF THE REQUIREMENTS FOR
THE DEGREE OF MASTERS OF SCIENCE IN MECHANICAL SYSTEM
DESIGN AND ENGINEERING**

**DEPATRMENT OF MECHANICAL AND AEROSPACE ENGINEERING
LALITPUR, NEPAL**

November 2023

COPYRIGHT

The author has agreed that the library, Department of Mechanical and Aerospace Engineering, Pulchowk Campus, Institute of Engineering may take this thesis freely available for inspection. Moreover, the author has agreed that the professor(s) who supervised the work recorded herein or, in their absence, by the Head of the Department wherein the thesis was done may be granted permission for extensive copying of this thesis for scholarly purpose. It is understood the recognition will be given to the author of this thesis and to the Department of Mechanical and Aerospace Engineering, Pulchowk Campus, Institute of Engineering in any use of the material of this report. Publication or copying or other use for financial gain without approval of Department of Mechanical and Aerospace Engineering, Pulchowk Campus, Institute of Engineering and author's written permission is prohibited.

Request for permission to copy or to make any other use of material in this report in whole or in part should be addressed to:

Head of the Department,

Department of Mechanical and Aerospace Engineering,

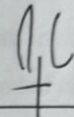
Pulchowk Campus, Institute of Engineering,

Lalitpur, Nepal.

**TRIBHUVAN UNIVERSITY
INSTITUTE OF ENGINEERING
PULCHOWK CAMPUS**

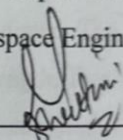
DEPARTMENT OF MECHANICAL AND AEROSPACE ENGINEERING

The undersigned certify that they have read, and recommended to the Institute of Engineering for acceptance, a thesis titled '**Design, Fabrication and Experimental Verification of Hypersonic Wind Tunnel with Manual Piston Driven Shock Tube. (A Table-Top Hypersonic Shock Tunnel)**' submitted by Akin Chhetri in partial fulfillment of the requirements for the degree of Msc. Mechanical Systems Design and Engineering.



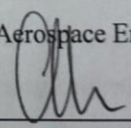
Prof. Laxman Poudel, Phd,

Supervisor,
Department of Mechanical and Aerospace Engineering



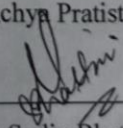
Asst Prof. Sudip Bhattarai, Phd,

Supervisor,
Department of Mechanical and Aerospace Engineering



External Examiner, Mr. Abhas Maskey, Phd,

Founder,
Antarikshya Pratisthan Nepal



Asst Prof. Sudip Bhattarai, Phd,

Committee Chairperson and Head of the Department,
Department of Mechanical and Aerospace Engineering



Date: 26/11/2023

ABSTRACT

A shock tunnel is a relatively low-duration wind tunnel made of a dump tank, test chamber, supersonic nozzle, and a shock tube. Ground-based hypersonic facilities are one of the most important setups for testing hypersonic flows. The study of hypersonic flows has expanded in many educational institute, but due to the high cost of experimental facilities, many institutions depend on theories and small scale CFD simulations to visualize hypersonic flows. Reddy Tunnel, which is one of the major inspirations of this paper, is a miniaturized hypersonic tunnel. Hence, this is an attempt to design, fabricate, and test an economic M6-free piston shock tunnel. The analytical calculations were done for the shock tube, nozzle and capacity of dump tank. The flow was considered isentropic and the simulations were done in OpenFoam v2112. The simulations showed the desired results in shock tube. The nozzle was axisymmetric and contoured. It was designed using method of characteristic in Matlab. The simulations of nozzle showed that it generated hypersonic speed of Mach number 5.2. The shock tube of 32 mm diameter was divided into two parts, where the length of the driver section was 510mm and the driven section was 490mm. The driven section was connected to a contoured supersonic nozzle of 295 mm length. Further, the nozzle was connected to a square test section of 150 x 150 x 200 mm dimensions. Finally, a dump tank of 300 x 400 mm dimension was attached to the test section. The experiment in the shock tube showed that ratio of flow velocity of incident shockwave was Mach number 1.59. The nozzle and test section assembly was joined to the shock tube and experiments were conducted with a test object in the test section. A single mirror Schlieren imaging showed an image formation of oblique shockwave and bow shockwave, which verified that the shock tunnel was operating in the boundaries of hypersonic speeds (Mach number 3 to 5). Furthermore, the development of this facility will help in testing different hypersonic flow over an object, it will also be beneficial in studying stagnant enthalpy, stagnation pressure, schlieren flow visualization etc. Another major aspects of this study will help the students studying compressible flows to have a basic idea of experimental hypersonics. In the future, by using the concepts of this shock tunnel, a larger shock tunnel could be designed and fabricated, which would have wider applications.

ACKNOWLEDGEMENT

I am grateful to the Department of Mechanical and Aerospace Engineering for providing the opportunity to do this project. I would like to thank my supervisors Prof. Laxman Poudel and Asst. Prof. Sudip Bhattacharai for mentoring me in this project. The expertise and technical knowledge they provided in the field of experimental and computational hypersonics was one of the major reasons for undertaking this project. Their mentorship and constant encouragement was invaluable to completing this project.

My extended thanks to Asst. Prof. Kamal Darlami, Head, Incubation, Innovation and Entrepreneurship Center for providing me a proper space and tools necessary to fabricate and install the shock tunnel. The setup in IIEC really helped me save a lot time and expenses.

I would also like to thank the Mechanical Workshop team of Pulchowk Campus. Lab in-charge Mr. Bal Shakya sir, Lab instructors, Mr. Chedi Sharma sir and Mr. Chandrika Prasad Adhikari sir for helping me during the fabrication processes. It would have been really difficult and expensive to complete this project without their help.

My gratitude to Research Engineer Mr. Nischal Poudel, who has worked parallelly with me in this project. His understanding of CFD simulations and hypersonic flows was a great addition to the armory and it really boosted the project. I would also like to extend my thanks to Research Engineers Mr. Nabin Bhandari and Miss Prativa Bhandari for their help during the experiment.

I am very thankful to my classmate Mr. Salim Maharajan who helped me during the Schlieren verification process. It was very tiring work, however his patience and enthusiasm in developing Schlieren technique was one of the major reason for the verification of this project.

I am grateful to Colonel Mukesh Batajoo sir and his team for helping me during the CNC machining of the Nozzle. It was one the most important part of this project and without the fabrication of Nozzle, this project would be incomplete.

Finally, I would like thank my classmates, especially Mr. Rakesh Chaudhary, who helped me during the initial material acquisition and many others who were insightful or helped to complete this project in different ways.

Contents

| | |
|--|-----------|
| COPYRIGHT | ii |
| ABSTRACT | iv |
| ACKNOWLEDGEMENT | v |
| List of Figures..... | ix |
| List of Tables | x |
| List of Abbreviations | x |
| CHAPTER 1 INTRODUCTION | 1 |
| 1.1 Background: | 1 |
| 1.1.1 Shock tube:..... | 1 |
| 1.1.2 Hypersonic Wind Tunnel:..... | 2 |
| 1.2 Research Gap: | 2 |
| 1.3 Problem Statement: | 2 |
| 1.4 Objectives: | 3 |
| 1.5 Scope: | 3 |
| 1.6 Limitation:..... | 3 |
| CHAPTER 2 LITERATURE REVIEW | 5 |
| 2.1 Free Piston Shock Tubes:..... | 5 |
| 2.2 Hypersonic Wind Tunnel:..... | 7 |
| 2.3 Basic Terminologies and Equations: | 8 |
| 2.3.1 Normal Shockwaves: | 8 |
| 2.3.2 Oblique Shockwaves:..... | 11 |
| 2.3.3 Bow Shockwave: | 12 |

| | |
|--|-----------|
| 2.4 Nozzle Theory:..... | 13 |
| 2.4.1 Equation for Flows in Nozzle: | 14 |
| 2.5 Method of Characteristics and Axisymmetric Nozzle: | 14 |
| 2.6 Shock Tube Theory:..... | 17 |
| 2.8 Operations of Shock tubes: | 20 |
| 2.9 High Speed Wind Tunnel Working Principle:..... | 21 |
| 2.10 Wind Tunnel Operation: | 23 |
| CHAPTER 3 METHODOLOGY | 24 |
| 3.1 Conceptual Framework: | 24 |
| 3.1 Literature Review: | 25 |
| 3.2 Analytical Calculations:..... | 25 |
| 3.3 Design and Modification: | 25 |
| 3.4 CFD Simulation: | 25 |
| 3.5 Material Selection and Instrument Acquisition: | 26 |
| 3.6 Fabrication: | 26 |
| 3.7 Calibration: | 26 |
| 3.8 Testing and Validation:..... | 26 |
| 3.9 Documentation and Presentation: | 26 |
| CHAPTER FOUR: ANALYTICAL CALCULATIONS, DESIGN AND FABRICATION | 27 |
| 4.1 Analytical Calculations:..... | 27 |
| 4.2 Modelling in CAD Software:..... | 29 |
| 4.3 Materials and Instruments:..... | 29 |
| 4.4 Design and Fabrication: | 30 |
| 4.5 Calibration and Experimental Setup: | 35 |

| | |
|---|-----------|
| 4.5.1 Calibration of the Shock tube: | 35 |
| 4.5.2 Calibration of the hypersonic wind tunnel:..... | 35 |
| 4.6 Schlieren Setup: | 35 |
| 4.7 Experimental Setup: | 37 |
| 4.8 Case Setup for Simulation: | 37 |
| 4.8.1 Shock tube:..... | 37 |
| 4.8.2 Nozzle: | 39 |
| Chapter 5 Result and Discussion | 42 |
| 5.1 Simulation Results of the Shock Tube:..... | 42 |
| 5.2 Simulation Results of the Nozzle:..... | 44 |
| 5.2.1 Mach Number in Nozzle: | 44 |
| 5.2.2 Static Pressure in Nozzle: | 46 |
| 5.3 Experimental Result of Shock tube: | 47 |
| 5.4 Experimental Results of Nozzle and Shock formation: | 48 |
| 5.5 Budget: | 51 |
| Chapter 6 Conclusion and Recommendation..... | 53 |
| 6.1 Conclusion: | 53 |
| 6.2 Recommendations:..... | 53 |
| References | 55 |
| APPENDIX I | 58 |
| APPENDIX II..... | 69 |

List of Figures

| | |
|---|----|
| FIGURE 1 SHOCK TUBE IN HANSON GROUP, STANDFORD | 1 |
| FIGURE 2 T4 STALKER TUBE..... | 2 |
| FIGURE 3 POST INCIDENT SHOCK TEMPERATURE AS FUNCTION OF DRIVER GAS PRESSURE AND DRIVER GAS TEMPERATURE | 5 |
| FIGURE 4 REDDY TUBE IN IISC BANGALORE, INDIA. | 6 |
| FIGURE 5 SCHEMATIC DIAGRAM OF REDDY TUNNEL..... | 8 |
| FIGURE 6 NORMAL SHOCKWAVE. | 9 |
| FIGURE 7 OBLIQUE SHOCKWAVE | 11 |
| FIGURE 8 BOW SHOCKWAVE..... | 12 |
| FIGURE 9 REQUIRED CONDITIONS FOR SUPERSONIC NOZZLE | 13 |
| FIGURE 10 CHARACTERISTIC LINE OF HYPERBOLIC FUNCTION DUE TO A POINT IN A FLOW FIELD..... | 15 |
| FIGURE 11 FLOW PROPAGATION IN A SUPERSONIC SPEED | 16 |
| FIGURE 12 DESIGN OF DIVERGENT SECTION OF THE NOZZLE USING MOC. | 17 |
| FIGURE 13 WORKING DIAGRAM OF A SHOCK TUBE | 19 |
| FIGURE 14 SHOCK WAVE PROPAGATION INSIDE A SHOCK TUBE..... | 21 |
| FIGURE 15 BLOW DOWN TYPE WIND TUNNEL..... | 22 |
| FIGURE 16 IN DRAFT WIND TUNNEL | 22 |
| FIGURE 17 PRESSURE-VACUUM TYPE WIND TUNNEL..... | 23 |
| FIGURE 18 FLOW CHART OF METHODOLOGY | 24 |
| FIGURE 19 ISOMETRIC VIEW OF 3D MODEL OF SHOCK TUNNEL. | 29 |
| FIGURE 20 FABRICATED SHOCK TUBE. | 31 |
| FIGURE 21 CONTOUR OF AXISYMMETRIC NOZZLE MAPPED OUT USING MOC IN MATLAB. | 32 |
| FIGURE 22 2D NOZZLE CONTOUR AFTER THE POINTS WERE IMPORTED IN A CAD SOFTWARE. | 32 |
| FIGURE 23 ISOMETRIC VIEW OF 3D MODEL OF AXISYMMETRIC NOZZLE. | 33 |
| FIGURE 24 (A) DIVERGING SECTION AND (B) CONVERGING SECTION OF NOZZLE..... | 34 |
| FIGURE 25 ISOMETRIC VIEW OF 3D MODEL OF DUMP TANK AND TEST SECTION ASSEMBLY..... | 34 |
| FIGURE 26 SCHLIEREN SETUP. | 36 |
| FIGURE 27 FINAL EXPERIMENTAL SETUP..... | 37 |
| FIGURE 28 DOMAIN DISCRETIZATION OF SHOCK TUBE | 38 |
| FIGURE 29 (A) DOMAIN DISCRETIZATION OF NOZZLE AND (B) BUTTERFLY GRID OF NOZZLE. | 40 |
| FIGURE 30 (A) STATIC PRESSURE CONTOUR AND (B) STATIC PRESSURE PLOT OF SHOCK TUBE AFTER INITIAL DIAPHRAGM BURST..... | 42 |
| FIGURE 31 (A) STATIC PRESSURE CONTOUR AND (B) STATIC PRESSURE PLOT OF SHOCK TUBE AFTER DEFLECTION..... | 43 |
| FIGURE 32 (A) MACH NUMBER CONTOUR AND (B) MACH NUMBER PLOT OF NOZZLE. | 45 |
| FIGURE 33 (A) STATIC PRESSURE CONTOUR AND (B) STATIC PRESSURE PLOT OF NOZZLE. | 46 |
| FIGURE 34 INITIAL DIAPHRAGM BURST OF SHOCK TUBE..... | 48 |
| FIGURE 35 (A) AND (B) SECOND DIAPHRAGM BURST OF SHOCK TUBE AND NOZZLE. | 49 |
| FIGURE 36 (A) AND (B) TEST OBJECT AND HIGH-SPEED CAMERA SETUP FOR SCHLIEREN IMAGING..... | 49 |
| FIGURE 37 (A) AND (B) SHOCKWAVE FORMATION IN TEST SECTION. | 50 |
| FIGURE 38 THETA-BETA-M PLOT AT (A) RAMP ANGLE 24 DEGREES AND WAVE ANGLE 32 DEGREE (B), RAMP ANGLE 24 DEGREE AND WAVE ANGLE 37 DEGREES AND (C) RAMP ANGLE 24 DEGREES AND WAVE ANGLE 45 DEGREES. | 51 |

List of Tables

| | |
|--|----|
| TABLE 1 DIMENSION OF OF THE NOZZLE. | 32 |
| TABLE 2 SOLVER SETUP OF SHOCK TUBE. | 38 |
| TABLE 3 SOLVER SETUP OF NOZZLE. | 41 |
| TABLE 4 ESTIMATED PRESSURE VALUES IN THE SHOCK TUBE AT DIFFERENT X/L RATIOS. (REDDY & SHARATH, MANUALLY OPERATED PISTON DRIVEN SHOCK TUBE, 2013) | 47 |
| TABLE 5 FINAL BUDGET OF THE PROJECT..... | 51 |

List of Abbreviations

γ = specific heat ratio $\frac{c_p}{c_v}$.

c_p = specific heat in constant pressure in $\frac{J}{kg\ K}$.

c_v = specific heat in constant volume in $\frac{J}{kg\ K}$.

M_1 = Upstream Mach number.

M_2 = Downstream Mach number.

p_1 = Pressure upstream of shockwave in Kpa.

T_1 = Temperature upstream of shockwave in Kelvin.

p_2 = Pressure downstream of shockwave in Kpa.

T_2 = Temperature downstream of shockwave in Kelvin.

$p_{0,1}$ = Total pressure upstream of shockwave in Kpa.

$T_{0,1}$ = Total temperature upstream of shockwave in Kelvin.

$p_{0,2}$ = Total pressure downstream of shockwave in Kpa.

$T_{0,2}$ = Total temperature downstream of shockwave in Kelvin.

V = Specific volume in $\frac{m^3}{kg}$.

dS = Infinitesimal area flux.

u_1 = Velocity in x-direction normal to the shockwave and upstream of shockwave in $\frac{m}{s}$.

u_2 = Velocity in x-direction normal to the shockwave and downstream of the shockwave

$\frac{m}{s}$. ρ = Local density of the fluid or object in $\frac{kg}{m^3}$.

ρ_1 = Density corresponding to p_1 in $\frac{kg}{m^3}$.

ρ_2 = Density corresponding to p_2 in $\frac{kg}{m^3}$.

e = Total internal energy in Joules (J).

h_1 = Enthalpy due to T_1 in $\frac{J}{kg}$.

h_2 = Enthalpy due to T_2 in $\frac{J}{kg}$.

ρ_0 = Total density in $\frac{kg}{m^3}$.

w_1 = Tangential velocity upstream of the shockwave.

w_2 = Tangential velocity downstream of the shockwave.

β = Wave angle in degrees (i.e. angle between shock wave and upstream flow direction).

$M_{n,1}$ = Upstream Mach number normal to the shock wave.

p_0 = Local total pressure in Kpa.

T_0 = Local temperature ratio in K.

dA = Differential area in the duct.

A = Area of the duct in m^2 .

A_1 = Area at the entry of the duct in m^2 .

A_2 = Area at the exit of the duct in m^2 .

A^* = Area at the throat of the nozzle in m^2 .

γ_1 = Specific heat ratio in driven section of the shock tube.

γ_2 = Specific heat ratio in the driver section of the shock tube.

M_s = Incident shock wave developed in the shock tube.

M_R = Reflected shock wave developed in the shock tube.

CHAPTER 1 INTRODUCTION

1.1 Background:

1.1.1 Shock tube:

The shock tube is a laboratory tool that can create varying flow speeds and regimes, commonly used for investigating shock waves. These waves result from the sudden release of energy, such as in explosions, volcanic eruptions, or from objects moving at supersonic or transonic speeds (usually above a Mach number of 0.3, as used by many scientists and engineers), as well as from high-speed projectiles and laser ablations. Shock waves are a ubiquitous occurrence in daily life and it has applications in diverse fields, from a simple gas stove combustion to complex areas like aerodynamics, biomedical science, chemical kinetics, and industrial processes. To study the effects of shock waves on different models, researchers developed shock tubes to generate controlled blasts and they examined it with the use various sensors. Shock tubes have been in use since 1899 when French scientist Paul Vielle invented the first compression-driven shock tube, but it was in the 1940s that interest in shock tubes were revived, and their use in research proliferated. As our knowledge of shockwaves has grown in recent times, so has their applications in a wide range of fields.



Figure 1 Shock tube in Hanson Group, Stanford

1.1.2 Hypersonic Wind Tunnel:

Hypersonic flows are the flow fields where the velocity is much larger than the velocity propagation of small disturbances, the velocity of sound (Tsien, 1946). Tsien was the first person to use the term 'Hypersonic'. The primary features of a hypersonic and high enthalpy flow are the high kinetic energy and the high stagnation temperature. After more than 60 years of research hypersonic ground test facility suitable for exploring aerothermochemistry still rely on high enthalpy shock tunnels (Jiang, Li, Hu, Liu, & yu, 2020). The T4 stalker tube in figure 2 was the first shock tunnel designed by Ray Stalker.

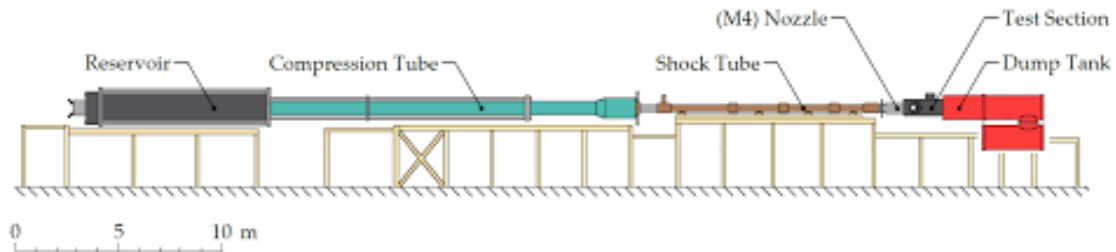


Figure 2 T4 Stalker tube

(J.Mee, Morgan, Paull, Jacobs, & Smart, 2017)

1.2 Research Gap:

Hypersonic has been a hotbed of research activities for many years now and ground based hypersonic facilities are one of the most important equipment to test the hypersonic object before developing an up-scaled model. This is an attempt to design and fabricate a miniature M6 hypersonic shock tunnel.

1.3 Problem Statement:

Hypersonic technologies have become increasingly important in the recent years. The study of hypersonic technologies has really expanded in many educational institutions over the years, but due the high cost of experimental facilities, many institutes rely on CFD simulations for research, while CFD is a powerful tool to recreate the physical model of the flow, it still requires proper meshing knowledge and high computational capacities, which can be expensive. Experimental setups give more accurate real world scenarios; nevertheless, errors in measurement and scaling of the model still exists. Reddy Tunnel, which is one of the major inspiration of this project, is a miniaturized hypersonic shock

tunnel. Likewise, this is an attempt to design, fabricate and test the Reddy tunnel by changing some major parts such as nozzle, shock tube, etc.

1.4 Objectives:

Main Objective:

To design, fabricate and test the Reddy tunnel by changing some the major parts such as nozzle, shock tube etc.

Specific Objective:

1. •To design using MOC in Matlab, simulate and fabricate an axisymmetric nozzle using CNC facilities available in Nepal.
2. •To use single mirror Schlieren technique to view the development of shockwave in the test section of the fabricated shock tunnel.
3. •To verify the pressure of the initial diaphragm burst in the shock tube using estimated values of X/L ratio given by KPJ Reddy. (Reddy & Sharath, Manually Operated Piston Driven Shock Tube, 2013).
4. To develop a more economical model of the Reddy tunnel.

1.5 Scope:

The scope of this study will be computational and experimental.

1.6 Limitation:

1. The shock tunnel was fabricated using local resources. As a result, there will be differences in dimensions, materials and design aspects of the shock tunnel, when compared to the Reddy tunnel. Therefore, a less accurate prototype would be made that could be enhanced later with proper time and budget.
2. The test time in the test section after the hypersonic tunnel will be very less in the order of 600 microseconds only.
3. The cylinder for the piston driven shock tube could not be honed properly as the honing tools required to machine the cylinder were not available. Hence, the boring of the cylinder was done using sandpaper, wooden mandrel and lathe. Therefore, the cylinder lacked in desired smoothness and uniformity.

4. A proper die was not available for machining a 300 mm nozzle in the CNC lathe facility available in Nepal. Hence, there were a few irregularities present in the Nozzle.

CHAPTER 2 LITERATURE REVIEW

2.1 Free Piston Shock Tubes:

As the name suggests design and fabricating a proper free piston shock tube is the first and one of the most important process in this project. To analyze the effects of temperature and driver gas effects, NASA Chemical Equilibrium with application (CEA) code provided the necessary information. This code has a "shock" option where the temperature and gas composition following incident shock in the shock tube could be studied. (Lynch, et al., 2019).

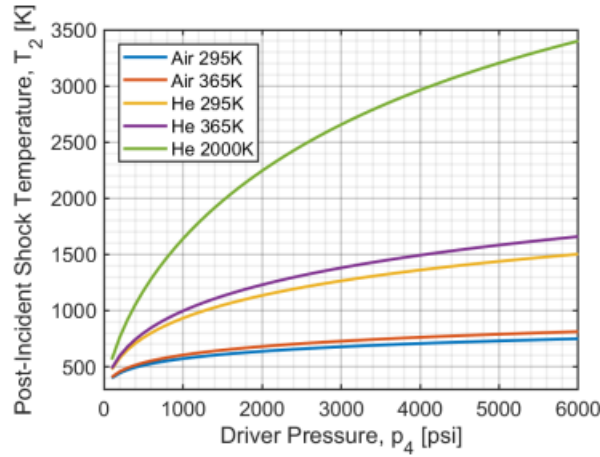


Figure 3 Post Incident Shock Temperature as Function of Driver gas pressure and Driver gas Temperature

(Lynch, et al., 2019)

If P_4 is considered as the pressure ahead of the piston in the driver section. Then from figure 3, we know that as the driver gas pressure increases, the post shock temperature also increases which ultimately results in developing a higher Mach number in the driven section. It could also be noted that air has the lowest increment in post shock temperature and helium has the highest increment in post shock temperature. Further, it also shows that if the driver gas is preheated then it helps in obtaining higher post shock temperature. In this experiment, we will use air as the driver gas for economical purposes even though helium shows the best results.

Manually operated shock tube developed in IISC Bangalore was the first of its kind to sustain a supersonic Mach number greater than 1.5 by using human force. It was noted that

driver gas pressure of 25 bar and 45 bar could be achieved by pushing the piston close to end of the compression tube while using air or helium as the driver gas (Reddy & Sharath, Manually Operated Piston Driven Shock Tube, 2013). This significantly reduced the volume of the driver gas required and the cost of operating a free piston shock tube. The Reddy tube uses a 30 mm diameter SS tube, which is not readily available in the local market. Therefore, in this experiment a 32 mm seamless MS tube will be used which is readily available in the market.

There will not be many changes as Mach number remains more or less constant varying only a maximum of 3% up to 46mm diameter (Kumar & Reddy, 2015). Air was be used in the driver and driven section and the specific heat ratios will be constant for both driver and driven section.



Figure 4 Reddy Tube in IISC Bangalore, India.

(Reddy, Hypersonic Flight and Ground Testing Activities in India, 2007)

2.2 Hypersonic Wind Tunnel:

A M6 (i.e Mach number 6) tunnel will be designed and fabricated for this experiment. They are basically a C-D nozzle with a fixed throat diameter. The conditions in upstream and downstream of the nozzle will be pre-determined. The boundary condition at the inlet of the nozzle will be determined by the stagnant pressure generated at the end of the driven section of shock tube while the boundary condition at the exit of the nozzle will be determined with the help of a vacuum pump attached to the dump tank. It is very important to maintain high pressure and temperature at the entry of the nozzle to achieve high Mach number at the exit of the nozzle.

At a speed of 2 km/s or at a sea level Mach number 6, the temperature at the stagnation point is 2400 K, and this is already at the limit of the regime where air may be considered, even approximately, as a perfect gas (HORNUNG, 1988) and as the test gas accelerates, the temperature decreases.

Typical hypersonic wind tunnels operate such that the static temperature in the test section approaches the liquefaction limit. As a result, the test section temperature for air is approximately 50 K. Also note if the stagnant temperature is equal room temperature at the entry of the nozzle one can achieve up to Mach number 5 (Bertin, 1994). Hence, to avoid liquefaction blankets or heater can be used or a proper stagnant temperature in the nozzle entry can be used.

The velocity of the contact surface will be greatly reduced as a consequence of the interaction with the primary reflected shockwave so that the flow duration, as limited by the arrival of the contact surface in the nozzle, will be substantially increased. This increased flow duration is, however, useful only if the disturbance created by the secondary reflected shock is too weak to significantly affect the uniformity of the flow entering the nozzle (Gai, 1992).

The freestream Mach number was observed to vary by 7.5 % from nozzle exit to the end of the test section, along the axial line. This increase is due to the conical flow exiting the nozzle into an unbounded form in the test section (Kumar & Reddy, 2015).

An experiment was conducted in the Reddy tunnel where the manual operation of piston was transformed into a pneumatic mode of operation. Hence, one of the major conclusion from that experiment was that higher thickness of metal diaphragm resulted in higher Mach flow number for identical test gas pressure but with the penalty of lower test time (Sudarshan, Pranav, & Sanjay, 2023).

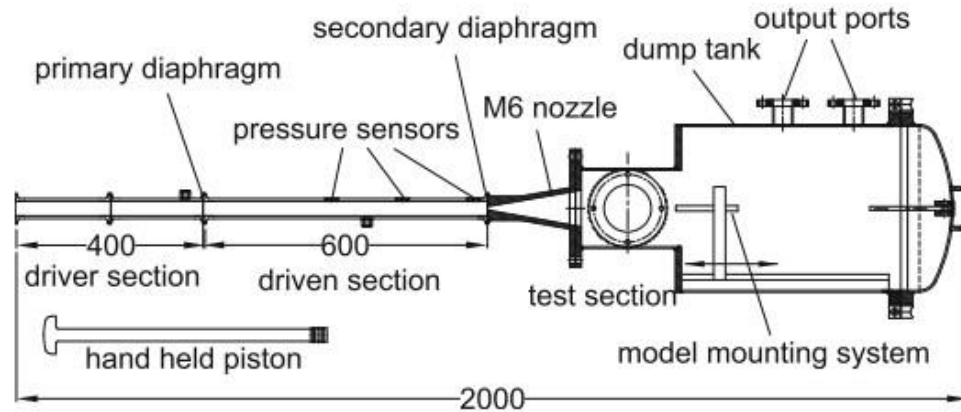


Figure 5 Schematic Diagram of Reddy Tunnel

(Kumar & Reddy, 2015).

2.3 Basic Terminologies and Equations:

2.3.1 Normal Shockwaves:

When the shockwave is perpendicular to the object, it is referred to as a normal shockwave. A normal shock is typically detached from the body and occurs when the flow is turned by a significant amount as shown in figure 6.

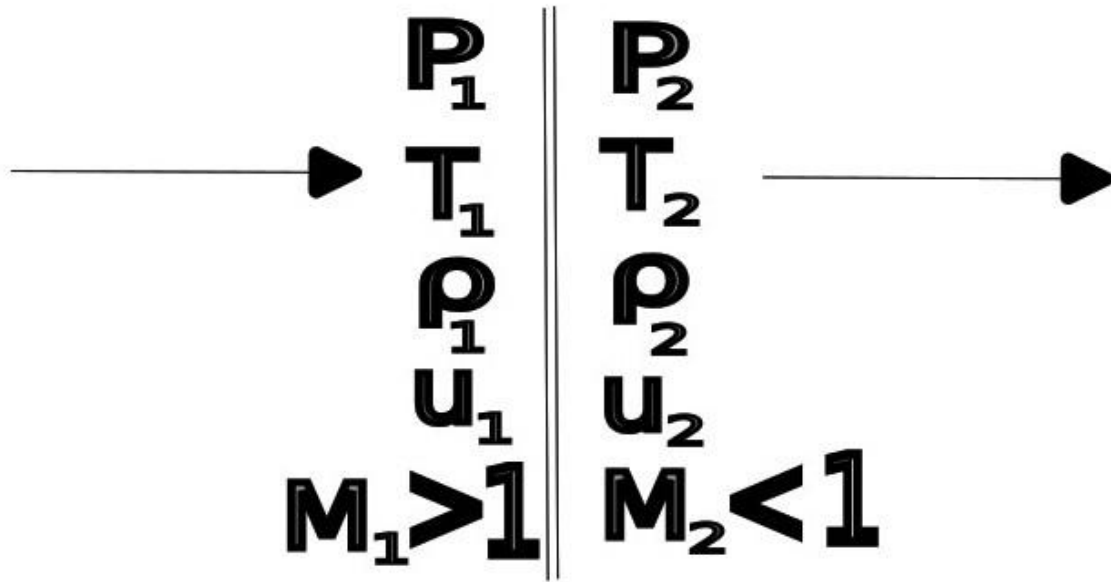


Figure 6 Normal Shockwave.

2.3.1.1 Governing Equations for Normal Shockwave:

The equations were taken from the book 'Fundamentals of Aerodynamics' (Anderson, 2017).

Continuity Equation in x-direction,

From the integral form of continuity equation,

$$\oint \rho \mathbf{V} \cdot d\mathbf{S} = 0 \quad (1)$$

The inflow will be negative and the outflow will be positive using the area vector sign convention.

$$\rho_1 u_1 = \rho_2 u_2$$

Momentum Equation in x-direction,

From the integral form of momentum equation,

$$\oint (\rho V \cdot dS) V = - \oint p dS \quad (2)$$

$$p_1 + \rho_1 u_1^2 = p_2 + \rho_2 u_2^2 \quad (3)$$

Energy equation in x-direction,

From the integral form of Energy equation,

$$\oint \rho \left(e + \frac{V^2}{2} \right) V \cdot dS = - \oint p V \cdot dS \quad (4)$$

$$h_1 + \frac{u_1^2}{2} = h_2 + \frac{u_2^2}{2} \quad (5)$$

Enthalpy,

$$h_2 = c_p T_2 \quad (6)$$

Equation of ideal gas,

$$p_2 = \rho_2 R T_2 \quad (7)$$

2.3.1.2 Normal Shockwave Relations:

Ratio of total conditions in a flow to the local conditions in a flow

i. Total temperature ratio to local temperature ratio,

$$\frac{T_0}{T} = 1 + \frac{(\gamma-1)M^2}{2} \quad (8)$$

ii. Total pressure ratio to local pressure ratio,

$$\frac{p_0}{p} = \left(1 + \frac{(\gamma-1)M^2}{2} \right)^{\frac{\gamma}{(\gamma-1)}} \quad (9)$$

iii. Total density ratio to local density ratio,

$$\frac{\rho_0}{\rho} = \left(1 + \frac{(\gamma-1)M^2}{2} \right)^{\frac{1}{(\gamma-1)}} \quad (10)$$

As, we can see all the ratios depend on γ and the local Mach number.

The equation below shows us the changes across the normal shockwave as a function of upstream Mach number M_1 only.

$$M_2^2 = \frac{1 + \left[\frac{\gamma-1}{2} \right] M_1^2}{\gamma M_1^2 - (\gamma-1)/2} \quad (11)$$

2.3.2 Oblique Shockwaves:

An oblique shockwave occurs when the shockwave is inclined to the direction of the flow displayed in figure 7.

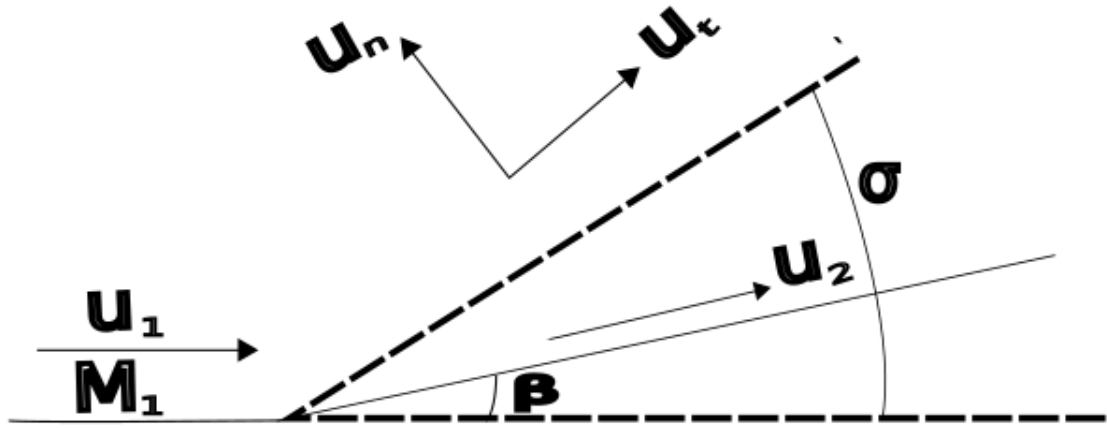


Figure 7 Oblique Shockwave

2.3.2.1 Governing Equations for Oblique Shockwaves:

Continuity equation and the energy equation will be same as in Normal Shockwave.

Momentum equation in x-direction,

$$\iint (\rho V \cdot dS) w = - \iint (P dS)_{\text{tangential}} \quad (12)$$

Hence,

$$- (\rho_1 u_1 A_1) w_1 + (\rho_2 u_2 A_2) w_2 = 0 \quad (13)$$

Dividing the obtained momentum equation by the obtained continuity equation for the oblique shockwave.

$$w_1 = w_2 \quad (14)$$

From the equation above, we can conclude that the tangential component of the flow velocity is constant across the shockwave.

$$p_1 + \rho_1 u_1^2 = p_2 + \rho_2 u_2^2 \quad (15)$$

This reveals that the normal components of the shockwave are solely accountable for the variations across the shockwave, and the tangential component does not have any effect. Consequently, the mathematical calculations employed in the normal shockwave will result in an equivalent equation for the oblique shockwave as well.

$$M_{n,1} = M_1 \sin \beta \quad (16)$$

We can see that the Mach number depends on two parameters M_1 and β unlike normal shockwave where it is depended on M_1 only.

2.3.3 Bow Shockwave:

If an oblique shock wave is anticipated to occur at an angle that cannot be sustained on the surface, a non-linear phenomenon emerges in which the shock wave forms a continuous pattern encircling the body as shown in figure 8, known as bow shocks. In such circumstances, the one-dimensional flow model is not applicable, and additional analysis is necessary to forecast the pressure forces exerted on the surface.

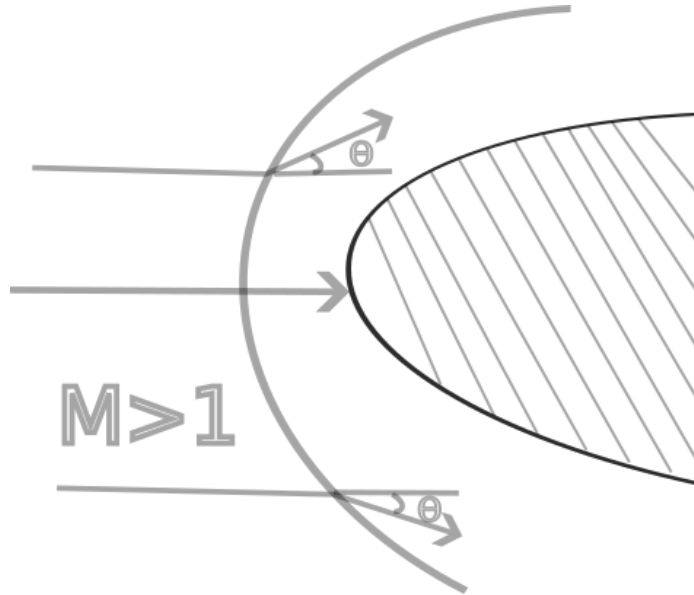


Figure 8 Bow Shockwave

2.4 Nozzle Theory:

Since, a convergent-divergent nozzle (C-D nozzle) will be attached at the termination of the driven section of the shock tube, it is crucial to grasp concept of fluid dynamics within the C-D nozzle. Nozzles have varying cross-sectional areas from inlet to outlet and an area-velocity relation is utilized to specify the Mach number within the nozzle.

$$\frac{dA}{A} = (M^2 - 1) \frac{du}{u} \quad (17)$$

If we study this relation closely, when du is positive the velocity increases and when du is negative the velocity decreases.

In subsonic flow ($M^2 - 1 < 0$),

Therefore, when area increases the velocity decreases and vice versa.

In supersonic flow ($M^2 - 1 > 0$),

Therefore, when area increases the velocity also increases and vice versa.

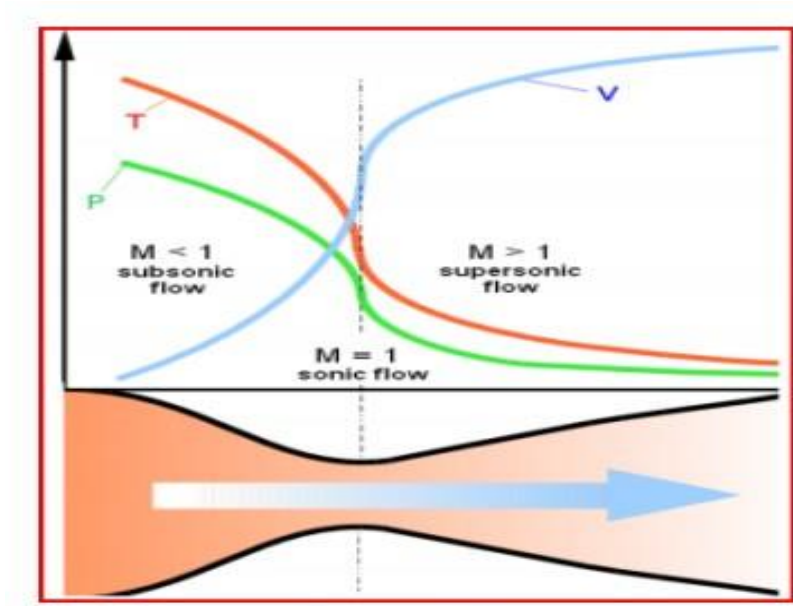


Figure 9 Required Conditions for Supersonic Nozzle

(Khan, Sardiwal, Sharath, & Chowdary, 2013)

2.4.1 Equation for Flows in Nozzle:

We will be using the same integral form of governing equation to determine the momentum of the flow. The pressure term added to the right is the pressure evaluated over the upper and lower surface of the control volume.

$$\oint (\rho \mathbf{V} \cdot d\mathbf{S}) \mathbf{V} = -\oint (p d\mathbf{S}) + \int_{A_1}^{A_2} p dA \quad (18)$$

$$p_1 A_1 + \rho_1 u_1^2 A_2 + \int_{A_1}^{A_2} p dA = p_2 A_2 + \rho_2 u_2^2 A_2 \quad (19)$$

The Area-Mach number used below is required to calculate the throat area and exit area for a particular exit Mach number.

$$\left(\frac{A}{A^*}\right)^2 = \frac{1}{M^2} \left[\frac{2}{\gamma+1} \left(1 + \frac{(\gamma-1)M^2}{2} \right) \right]^{\frac{(\gamma+1)}{(\gamma-1)}} \quad (20)$$

2.5 Method of Characteristics and Axisymmetric Nozzle:

An axisymmetric nozzle is a three dimensional nozzle. Unlike a two dimensional planar nozzle, an axisymmetric nozzle does not have corners which negates the formation of vortices, resulting in higher quality flow. Although, axisymmetric nozzles are not commonly used in wind tunnel facilities, they are commonly used in rocket propulsion. (Uyeki, 2018)

In a nozzle with supersonic speed at the exit, the convergent section will always have subsonic speed. Hence, the losses in the convergent section will be comparatively less than the divergent section. Therefore, the convergent section of this nozzle is linear. Due to the high losses in the divergent section, the divergent section will be designed using Method of Characteristics (MOC).

Solving the flow fields analytically is very challenging but due to the hyperbolic nature of supersonic flows, they have a certain characteristic that information propagates in certain directions which are known as characteristic lines. Previously, Velocity potential equation and small perturbation methods were used to solve the hyperbolic partial differential equation.

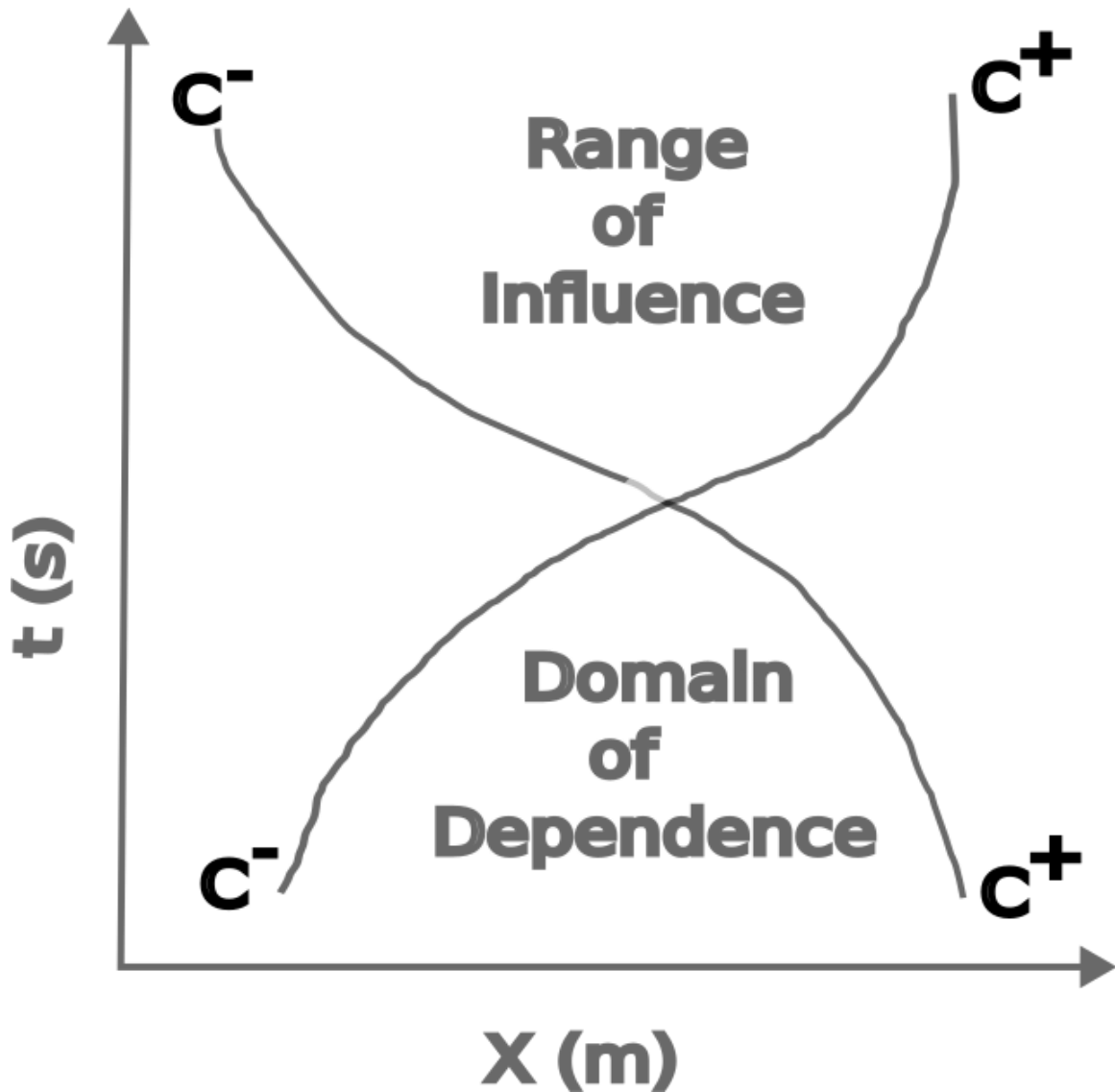


Figure 10 Characteristic line of Hyperbolic function due to a point in a flow field.

Any particular point in a hyperbolic equation or hyperbolic flow, the solution of that point is influenced by all the region which are bounded by two characteristics line, C^+ and C^- as shown in figure 10. The region bounded by the two characteristics which influences a particular point in the domain is known as dependence of domain. The particular point is dependent on initial values that are bounded by the two characteristics which passes through that particular point. When the characteristics of the point is pushed ahead, the point influences all other point ahead of it only along certain direction which are bound the characteristic curve.

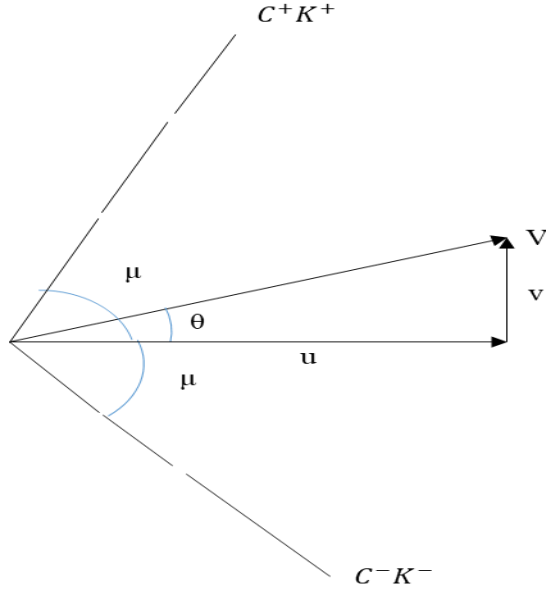


Figure 11 Flow propagation in a supersonic speed

From figure 11, consider a x-velocity as u and y-velocity as v . Such that their component is V at an angle θ . Two waves are at an angle μ with respect to that point so that the solution propagates along Mach wave. From the figure, it is known that the solutions are located at $(\theta \pm \mu)$. Hence, the slope of characteristic lines is given by,

$$\frac{dy}{dx} = \tan (\theta \pm \mu) \quad (21)$$

where, μ is the Mach angle.

| Characteristic lines | Slope | | Compatibility Condition |
|----------------------|-----------------------|-------|-------------------------------|
| C^- | $\tan (\theta - \mu)$ | K^+ | $\theta + \vartheta(M) = K^-$ |
| C^+ | $\tan (\theta + \mu)$ | K^- | $\theta - \vartheta(M) = K^+$ |

Table 1 Equation for solving Characteristics lines and Compatibility Condition.

Where,

$\vartheta(M)$ = Prandtl-Meyer function.

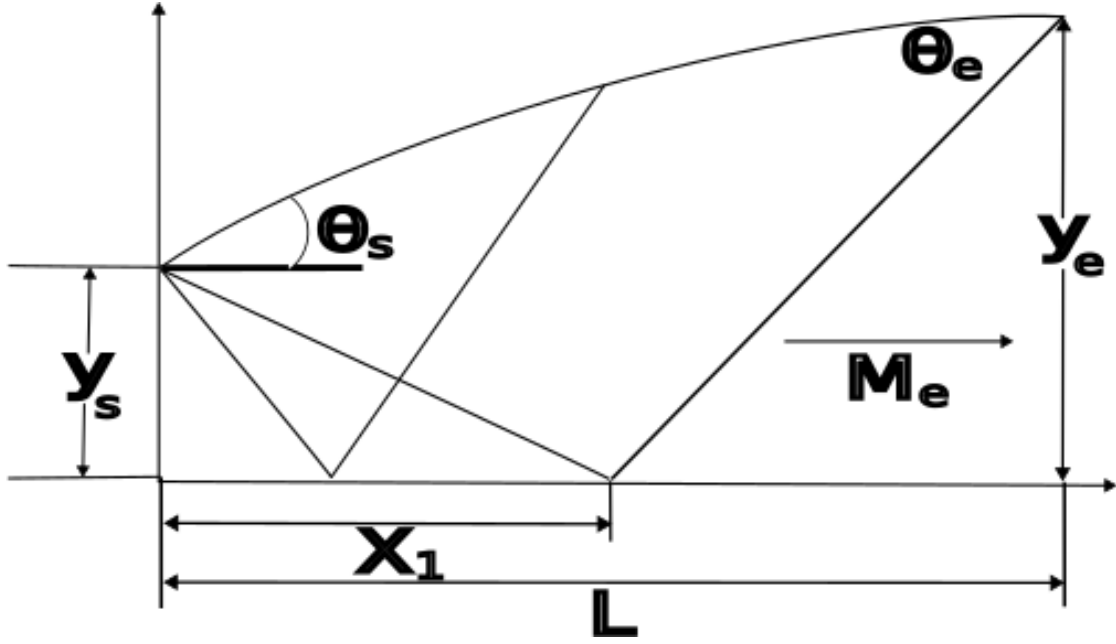


Figure 12 Design of Divergent Section of the nozzle using MOC.

As shown in figure 12 the characteristics lines are drawn along the nozzle wall. The exit and throat Mach number are already known. Hence, the characteristic and compatibility of each wave is solved using the equations in Table 1.

The use of MOC is one of the most effective ways to design a nozzle, as the flow in the divergent section designed using MOC for a particular net pressure ratio showed no sign of shockwave formation. Whereas, off design condition generated oblique shockwave and expansion fan reducing the nozzle performance (Ranabhat, Darlami, Bhattarai, & Shrestha, 2022). Further, the use of MOC is an essential feature to achieve steady sustained supersonic flow (Khan, Sardiwal, Sharath, & Chowdary, 2013).

2.6 Shock Tube Theory:

The discussion on shock tube theory is limited to compressed-gas-driven-type shock tube having a circular cross section. The relationship between the thermodynamic properties on both sides of the shock front is given by the Rankine–Hugoniot relations which is also known as the jump conditions (Vivek & T.G.Sitharam, 2019). The flow inside the tube is assumed to be ideal gas with constant specific heat and inviscid. The governing equations for the conservation of mass, momentum, and energy are similar to those of normal shock waves.

$$\frac{T_2}{T_1} = \frac{p_2}{p_1} \left(\frac{\frac{\gamma+1}{\gamma-1} + \frac{p_2}{p_1}}{1 + \frac{\gamma+1}{\gamma-1} \frac{p_2}{p_1}} \right) \quad (22)$$

$$\frac{\rho_2}{\rho_1} = \left(\frac{\frac{\gamma-1}{\gamma+1} + \frac{p_2}{p_1}}{\frac{\gamma-1}{\gamma+1} \frac{p_2}{p_1} + 1} \right) \quad (23)$$

Similarly, pressure ratio across the shockwaves depends upon the Mach number of incident shockwave.

$$\frac{p_2}{p_1} = 1 + \frac{2\gamma(M_s^2 - 1)}{\gamma + 1} \quad (24)$$

Thus, we can utilize the aforementioned known properties to calculate the Mach number, M, using the following equation.

$$\frac{p_4}{p_1} = \frac{\gamma_1 - 1}{\gamma_1 + 1} \left[\frac{2\gamma_1(M_s^2 - 1)}{\gamma_1 - 1} \right] \left[1 + \frac{\gamma_4 - 1}{\gamma_4 + 1} \left(\frac{a_1}{a_4} \right) \left(M_s - \frac{1}{M_s} \right) \right]^{\frac{-2\gamma_4}{\gamma_4 - 1}} \quad (25)$$

Using the Mach number of the incident shock wave obtained above, we can find the Mach number of the reflected shockwave.

$$\frac{M_R}{M_{R-1}} = \frac{M_s}{M_{s-1}} \sqrt{1 + \left(\frac{2(\gamma_1 - 1)}{(\gamma_1 + 1)} (M_s - 1) \left(\gamma_1 + \frac{1}{M_s^2} \right) \right)} \quad (26)$$

2.7 Piston Driven Shock Tube Working Principle:

The shock tube consists of 2 main parts: -

i. Driver Section

ii. Driven Section

A diaphragm separates two sections, namely the driver section and the driven section. The driver section is pressurized by pushing the piston and compressing a high-velocity gas such as nitrogen, helium, etc. Once the diaphragm is ruptured, high-pressure gas is suddenly released into the low-pressure driven section at $t = 0$, causing a series of compression waves to propagate into the driven section. These compression waves raise

the temperature of the driven gas. The compression waves at the high-temperature region travel faster than the pressure waves and eventually converge to form a shockwave. The formed shockwave travels faster than the velocity of sound in the driven gas. When the driver gas and driven gas come in contact with the contact surface, expansion waves are formed, which travels in the opposite direction to the shockwave into the driver section displayed in figure 13.

These expansion waves travel at the speed of sound, and the pressure in driver section drops gradually. Once the expansion wave reach the end of the driver section, the head of the expansion wave gets reflected and interacts with the incoming tail part of the expansion wave, which further accelerates the expansion wave into the driven section. The shockwave travels to the end of the driven section and gets reflected, further aiding the pressure rise in the driven section. Finally, the expansion waves and the reflected shockwave interact with each other in the driven section, which aids in the decay of the shockwave.

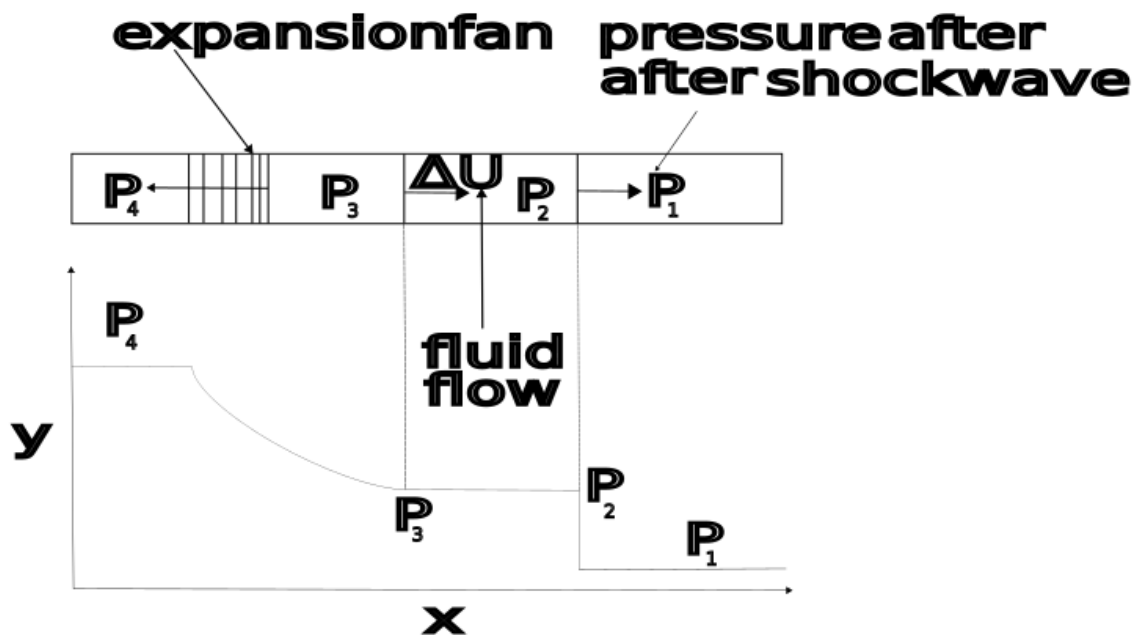


Figure 13 Working Diagram of a Shock Tube

2.8 Operations of Shock tubes:

On the basis of wave profile, shock tubes can be operated in 2 ways:

i.Shock wave

ii.Blast wave

The distinction between shock wave and blast wave is the presence of a shock front in the shock wave profile, characterized by a sudden jump, followed by a contact surface pressure that remains constant for a certain time. A driving force is necessary to generate a shock wave, and the sudden release of a driver gas inside the shock tube aids in its formation. As shown in figure 14, the reflected expansion waves intercept the reflected shock waves, reducing the pressure levels.

Increasing the length of driver section and using a driver gas with a lower speed than that of sound helps in delaying the development of the expansion waves. In the blast wave profile reflected expansion waves catch the incident shock wave instead of the reflected shockwave. This is accomplished by reducing the length of the driver section compared to that of the shockwave profile and using a gas with a speed greater than the speed of sound. The shortened driver section reduces the time, expansion wave needs to travel in the driver section, and the gas with a velocity greater than the speed of sound assists the expansion wave in accelerating faster into the driven section after it crosses the contact surface. The pressure decay takes place before the shockwave is reflected, and the incident shockwave pressure is significantly decreased. Shock wave profile generation can be used to study the shock loading, which is similar to the hammering effect and blast wave profile generated can be used to study the blast loading, which is caused due to explosion.

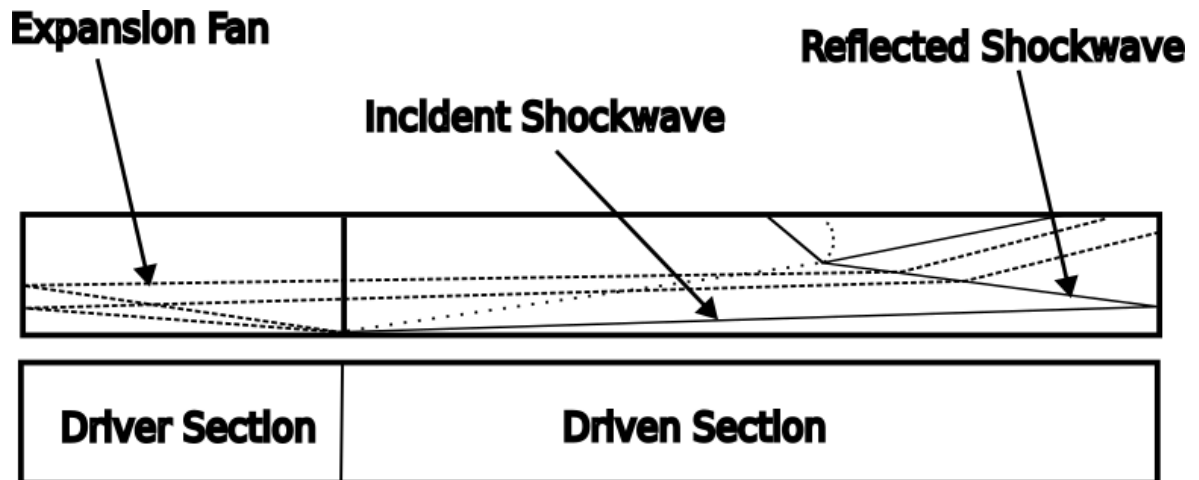


Figure 14 Shock Wave Propagation inside a Shock Tube.

2.9 High Speed Wind Tunnel Working Principle:

The high-speed wind tunnels can be sub-divided in two broad categories: -

1. Continuous facilities.
2. Intermittent facilities.

A continuous facility is a closed wind tunnel; the test section will have flows at least above Mach number 1.

$$P \sim \frac{1}{2} \rho u^2 A \cdot u \quad (27)$$

From the above equation of power, we can see that the velocity is in the cubic order (i.e. u^3). Hence, for very high speed we can conclude that the power requirement is going to be very high and continuous.

The major advantage of these facilities is that the test time is greater.

Nevertheless, these wind tunnels are very expensive to operate and maintain in most of the labs. Therefore, only a few of these have been built with high funding and separate power station.

On the other hand, intermittent facilities store the energy and deliver it all at once and then the process is repeated again. There are mainly three types of intermittent wind tunnel: -

1. Blow Down type.
2. In draft type.
3. Pressure-vacuum type.

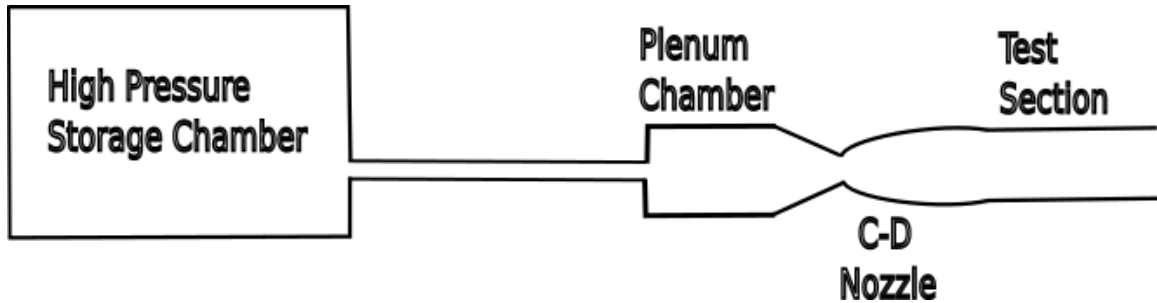


Figure 15 Blow Down Type Wind Tunnel

As shown in figure 15 in the blow down type intermittent wind tunnel, air is stored in high-pressure tank at high pressure over long duration of time. This, ensures that the compression is done effectively like the phenomenon of rechargeable batteries. Further, the flow is passed through the C-D nozzle at very high pressure when required; the downstream of the nozzle will be kept at ambient conditions.

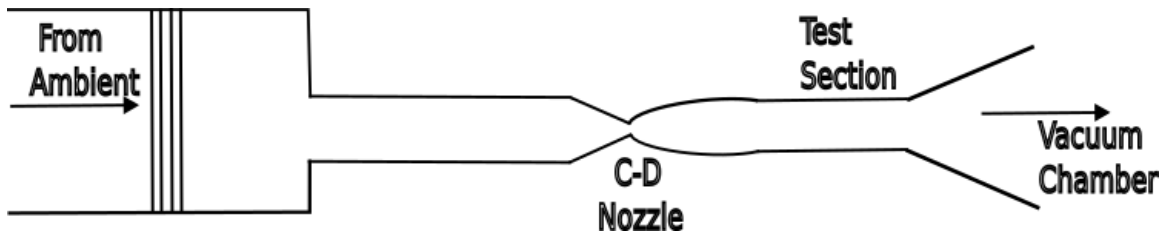


Figure 16 In draft Wind Tunnel

The indraft type intermittent wind tunnel is shown in Figure 16 where the operation of the tunnel is in contrast to the blow down wind tunnel, but the working principle is same. We will maintain a low pressure downstream of the nozzle in the vacuum chamber using a vacuum pump. The inlet at the upstream of the nozzle will be at ambient conditions.

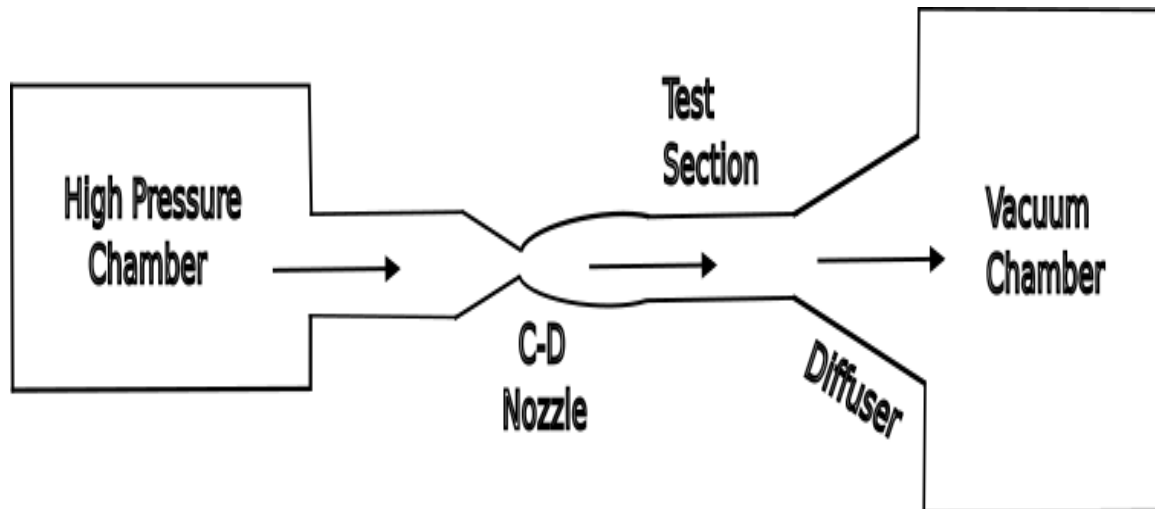


Figure 17 Pressure-Vacuum Type Wind Tunnel

(Rose, Jinu, & Brindha, 2015)

Figure 17 shows a pressure-vacuum type intermittent wind tunnel, which will use both high-pressure tank upstream of the nozzle and vacuum/low pressure tank downstream of the nozzle. Shock tunnel is also a type of pressure-vacuum tunnel.

2.10 Wind Tunnel Operation:

The stagnant pressure due to the impact of shock wave in the driven section is used as inlet pressure or the boundary condition that enters the nozzle. The speed of the flow will be subsonic for the entire convergent section. The gas from the entry of the nozzle flows to the throat where choking occurs i.e. $M \geq 1$. The throat size for choking to occur are calculated in the analytical calculations below. When the speed of the flow reaches just above Mach 1 at the throat, the divergent part of the nozzle expands the gas/air such that it moves at high speed to the annular opening of the nozzle to maintain the momentum equation. The pressure in the divergent section is very low compared to high-pressure region of the convergent section and hence, the velocity rapidly increases.

The gas flows from the nozzle into the test section, which may affect the Mach number to some extent. The test section is further connected to the dump tank where vacuum pump is preset to a certain absolute pressure making the shock tunnel pressure-vacuum type.

CHAPTER 3 METHODOLOGY

3.1 Conceptual Framework:

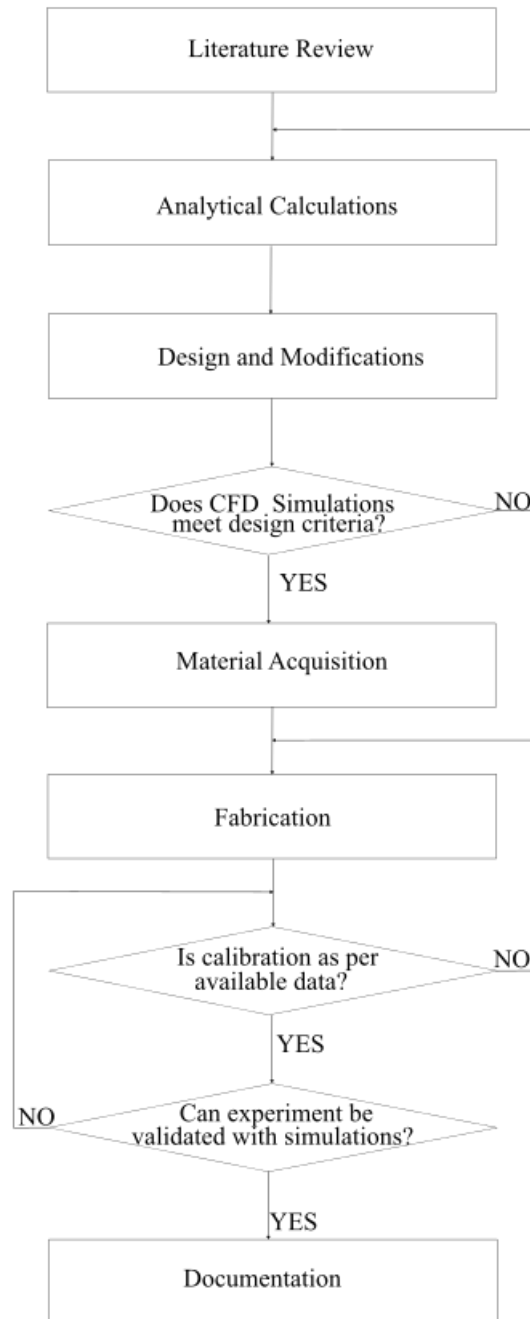


Figure 18 Flow Chart of Methodology

3.1 Literature Review:

The Literature Review was done from various sources such as books, articles, journals, and papers written for compressible flows and high-speed wind tunnels. Fundamentals of Aerodynamics written by John D Anderson was used to write the equations in the literature review. The most important task of the literature review was to understand the concept of compressible flows, shock waves and high-speed wind tunnels. One of the major source of the literature in this thesis was the work of Dr. KPJ Reddy who was the inventor of manual piston driven shock tunnel.

3.2 Analytical Calculations:

The analytical calculations were done before the design and simulation of the shock tube and nozzle. At the exit, Mach number 6 set as target outlet condition for this thesis. The design and calculations were done for the aforementioned Mach number. The nozzle exit area was $5.026 \times 10^{-3} \text{ m}^2$. Similarly, calculations for the shock tube was done for its design. The pressure ratios at different region in shock tube where the shock propagates were calculated. The temperatures of the same region was also calculated. Finally, the vacuum pump capacity was calculated.

3.3 Design and Modification:

The Design of the nozzle was done using MOC with a code written in Matlab. Similarly, the material required for the completion of this project was finalized and according to the analytical calculations, the equipment and vessels were designed in a CAD software. The length of the shock was taken in reference to the Reddy Tube while the diameter of the shock tube decided as per the availability of seamless MS tubes in the local market. The dump tank and test section were designed with reference to Reddy Tunnel. While the window in the test section was designed with reference to Schlieren setup available in the campus premises.

3.4 CFD Simulation:

The CFD simulations were done in OpenFoam v21122. Openfoam is a widely used open source software, mostly used for simulations of fluid engineering domain. OpenFoam solver rhoCentralFoam was used to simulate Mach number and static pressure conditions of the shock tube and nozzle for this thesis.

3.5 Material Selection and Instrument Acquisition:

Most of the material used for this project was Mild Steel. As, it was cheaper and it has higher ductility compared to stainless steel. Even though the hardness of Mild steel is less compared to the stainless steel. Due to the availability of mild steel in the local market it was easier to acquire Mild steel materials and it's fabricators. Other materials used were GI nut and bolts, red oxide, paint, Acrylic glass, copper etc.

3.6 Fabrication:

A shock tube was fabricated with help of trained welder and fabricators. The dump tank and test section were fabricated in a workshop with rolling machine.

3.7 Calibration:

The calibration of the shock tube and hypersonic tunnel will be as per the data available for the Reddy tube and Reddy Tunnel experiments in IISC Bengaluru.

3.8 Testing and Validation:

The testing of the hypersonic tunnel was done with help single mirror schlieren imaging. A shockwave pattern was seen and using the theta-beta-M plot, the Mach number of the shockwave was validated. However, for proper verification of Mach number 6, a 10 KHz pressure transducer is required, which needs to be imported.

3.9 Documentation and Presentation:

After the successful completion of all the methods, the research study was systematically documented and it was submitted to Department of Mechanical and Aerospace Engineering.

CHAPTER FOUR: ANALYTICAL CALCULATIONS, DESIGN AND FABRICATION

4.1 Analytical Calculations:

i. Throat Area of the nozzle:

Considering $M_e = 6$,

$$\gamma = 1.4,$$

Target exit Area,

$$A_e = 5.026 \times 10^{-3} \text{ m}^2.$$

From gas tables for compressible flows we have, 5.026,

for $M_e = 6$,

$$\frac{A_e}{A^*} = 53.180,$$

Considering $A^* = 9.519177 \times 10^{-5} \text{ m}^2$,

We get throat diameter $d_t \approx 11 \text{ mm}$.

ii. Pressure in the driven section of the shock tube before diaphragm bursts:

$$p_4 = p_1 \left(\frac{X}{L} \right)^{-\gamma} \quad (28)$$

We put initially $p_1 = 1 \text{ atm}$,

We get, $p_4 = 952 \text{ Kpa}$,

If $\frac{X}{L} = 0.2$, the $\frac{X}{L}$ ratio can change according to the strength of the person pushing the piston.

Hence, we will get different pressures up to 2500 KPA with air accordingly.

iii. Incident Shock Wave:

The incident Shock wave obtained using shock tube relations and pressure ratios $\frac{P_4}{P_1}$ is

$M_s = 1.59$ which can rise up to 1.90 with maximum pressure ratio.

Considering,

$$T_4 = T_1 = 300 \text{ K at room temperature and}$$

$$R = 287 \frac{J}{Kg.K}.$$

iv. Pressure after the contact surface of the shock tube:

Using the known value of M_s and p_1 we get,

$$\frac{p_2}{p_1} = 2.7827,$$

$$p_2 = 282.696 \text{ Kpa.}$$

v. Pressure reflected at the end of shock tube:

Using the relation,

$$\frac{p_5}{p_1} = \left[\frac{2\gamma_1 M_s^2 - (\gamma_1 - 1)}{\gamma_1 + 1} \right] \times \left[\frac{(3\gamma_1 - 1)M_s^2 - 2(\gamma_1 - 1)}{(\gamma_1 - 1)M_s^2 + 2} \right] \quad (29)$$

Therefore, $p_5 = 681.674 \text{ Kpa.}$

vi. Temperature due to reflected shockwave:

Using the relation,

$$\frac{T_5}{T_1} = \frac{\left[\frac{\{2\gamma_1 M_s^2 (\gamma_1 - 1) + (3 - \gamma_1)\}}{\times \{M_s^2 (3\gamma_1 - 1) - 2(\gamma_1 - 1)\}} \right]}{\{M_s^2 (\gamma_1 + 1)^2\}} \quad (30)$$

Therefore, $T_5 = 543 \text{ K.}$

vii. Vacuum pump capacity:

For Vacuum Pump Calculations to maintain a pressure of 42000 Kpa:-

$$P_I V_1 = P_F V_2 \quad (31)$$

Tank dimension: - diameter = 300mm, height = 400 mm,

Volume of the tank = $\pi r^2 h$,

$$V_1 = 0.0282 \text{ m}^3.$$

$$P_I = 101325 \text{ pascal or 1 atm,}$$

$$P_F = 42000 \text{ Kpa,}$$

$$V_2 = 0.0683 \text{ m}^3 = 68.3 \text{ ltr.}$$

4.2 Modelling in CAD Software:

The CAD drawings were made in SolidWorks 2020 as shown in figure 19.

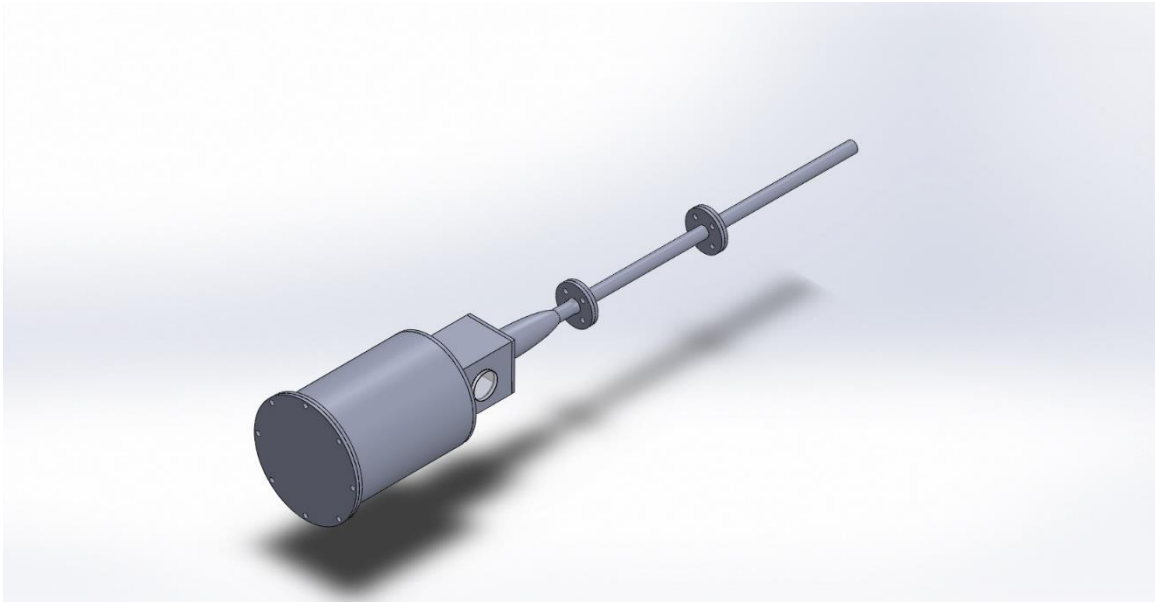


Figure 19 Isometric View of 3D model of Shock Tunnel.

4.3 Materials and Instruments:

i. MS tubes and MS rod:

MS tubes used in this project was manufactured by Jindal Steel. As, mentioned before the diameter of the tube was 32 mm. Seamless tubes were used for smooth operation of shock tube. Similarly, MS rod of 40 mm was used to fabricate the piston.

ii. MS flanges:

A MS flanges of 32 mm was used to join the driver and driven section of the shock tube. The driven section and the nozzle inlet of the shock tunnel was also joined using the flange of same size.

Furthermore, MS flange of 65 mm was mounted on the external wall of the nozzle and at the inlet of the test section. Finally, a 300 mm MS flanges and a dummy flange of the same specification was used to enclose the exit of the tank, which also worked as a maintenance hatch for the tank.

iii. Rubber Gasket:

A Rubber gasket of the required size was kept in between the flanges to avoid leakages.

GI nuts and bolts:

GI nuts and bolts of size M19 was used to screw the flanges together to connect different sections of shock tube, nozzle and dump tank.

iv. Pressure gauge:

The pressure gauge of 2MPa was used at the end of driver section to measure the stagnant pressure before the diaphragm is burst.

v. Red oxide, paint and sand paper:

The Mild Steel material is susceptible to rusting, therefore the outer part of the MS materials were painted with red oxide and a blue paint. Sand paper of medium and coarse grade was used to smoothen the inside and outside of the fabricated shock tunnel.

vi. Vacuum Pump:

An i-Rex double stage oil type vacuum pump was used to create absolute pressure in the dump tank. The free air displacement of the pump was 11.8 CFM and the ultimate vacuum capacity of the pump was 1.99 pascal.

4.4 Design and Fabrication:

1. Shock Tube:

As this paper follows the Reddy tube, the length of the shock tube was unchanged. The tube was drawn and designed in a CAD software. It was then simulated with help of OpenFoam v2112, which had a tutorial case of shock tube. The details of the simulations are presented in the later chapters. The fabricated shock tube is displayed in figure 20.

The 32 mm flange was arc welded at one end of the driver section and at the both ends of driven section. The welding was done by a trained welder in a local workshop. A hole of 10 mm was drilled at the end of the driver section and a threaded MS socket of 15 mm was welded with the hole in the center to accommodate the pressure gauge. Furthermore, the

rubber gasket was cut to the precise shape and size of the flanges and then the flanges were bolted together with rubber gasket in between to avoid leakage.



Figure 20 Fabricated Shock Tube.

2. Convergent-Divergent Nozzle:

The convergent and divergent nozzle was of axisymmetric shape and it was designed using MOC as shown in figure 21. The base code was written by Ludovico Fossa in MATLAB and it was posted in 2021 in math works. This code was further edited in MATLAB R2023 student version and the nozzle contour was imported to a CAD software as shown in figure 22.

Axisymmetric minimum-length nozzle contour

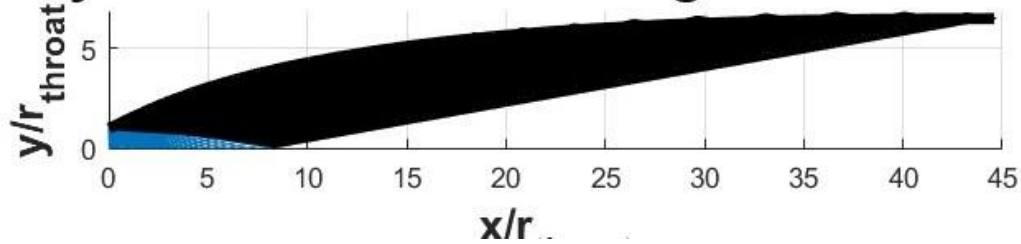


Figure 21 Contour of Axisymmetric Nozzle Mapped Out using MOC in MATLAB.

There were about 187 points generated through this code in x and y direction. The points in the x-axis started from 0 at the throat and terminated at 44.5. This represented the length of the nozzle. While the points in y-axis started from 1 at the throat and terminated at 6.49. This represented the half height of the nozzle. As the nozzle was axisymmetric the points could be mirrored across y-axis. The points were multiplied by 5.5 to match the analytical calculation for this project. The multiplication of the points resulted in the following changes in the nozzle dimension.

| | | | |
|------------------|-------------|-----------------------|-------------|
| Length at throat | 0 mm | Half height at throat | 5.5 mm |
| Length at exit | 245.2112 mm | Half height at exit | 35.70356 mm |

Table 1 Dimension of of the Nozzle.



Figure 22 2D nozzle contour after the points were imported in a CAD software.

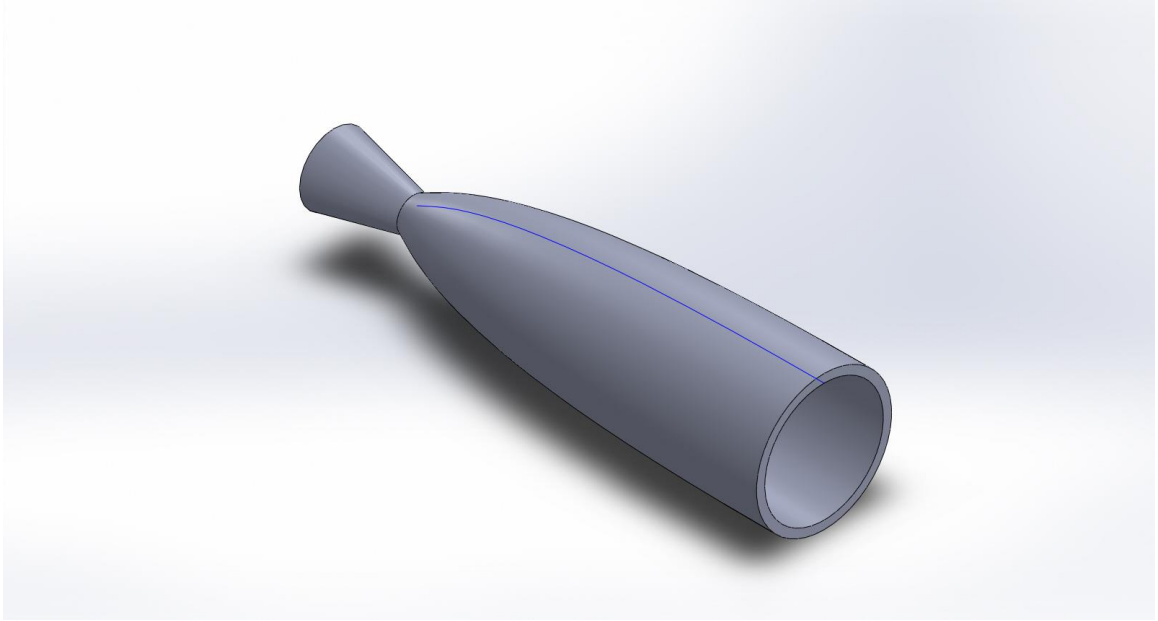


Figure 23 Isometric View of 3D Model of Axisymmetric Nozzle.

The nozzle design was given for CNC lathe machining. A three dimensional nozzle was designed in a CAD software as shown in figure 23. It was further manufactured using CNC lathe machine pictured in figure 24(a) and figure 24(b). As it was clearly seen from the figure that there were irregularities present in the internal walls of converging and diverging section of the nozzle, which might have affected the flow.

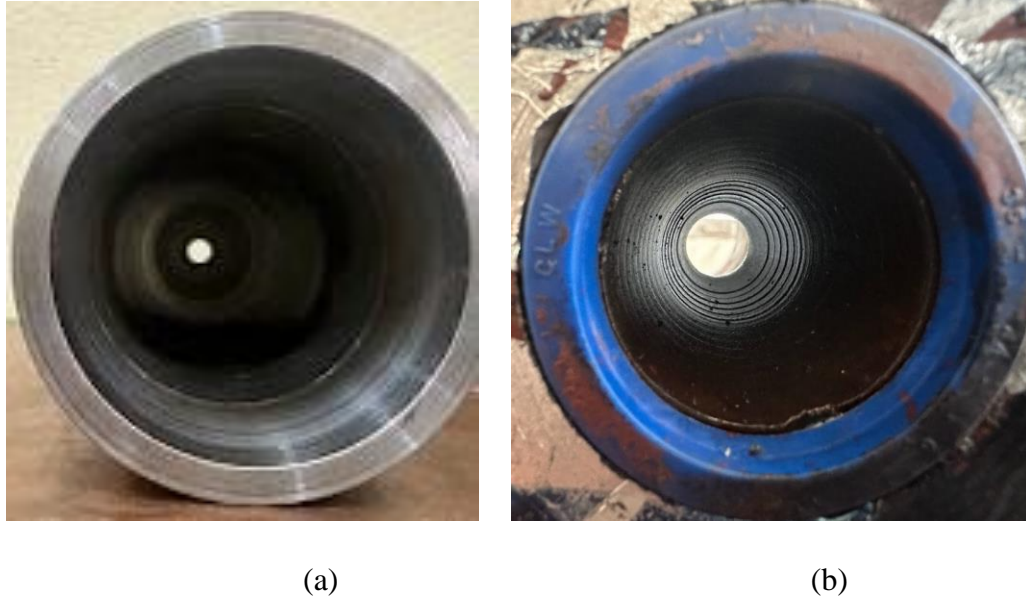


Figure 24 (a) Diverging section and (b) converging section of Nozzle.

3. Dump Tank and Test Section:

The dimension of the dump tank was 300X400 mm. Similarly, the dimension of the test section is arbitrary 150X150X200 mm. The dump tank and test section assembly were first drawn and designed in a CAD software as shown in figure 25.

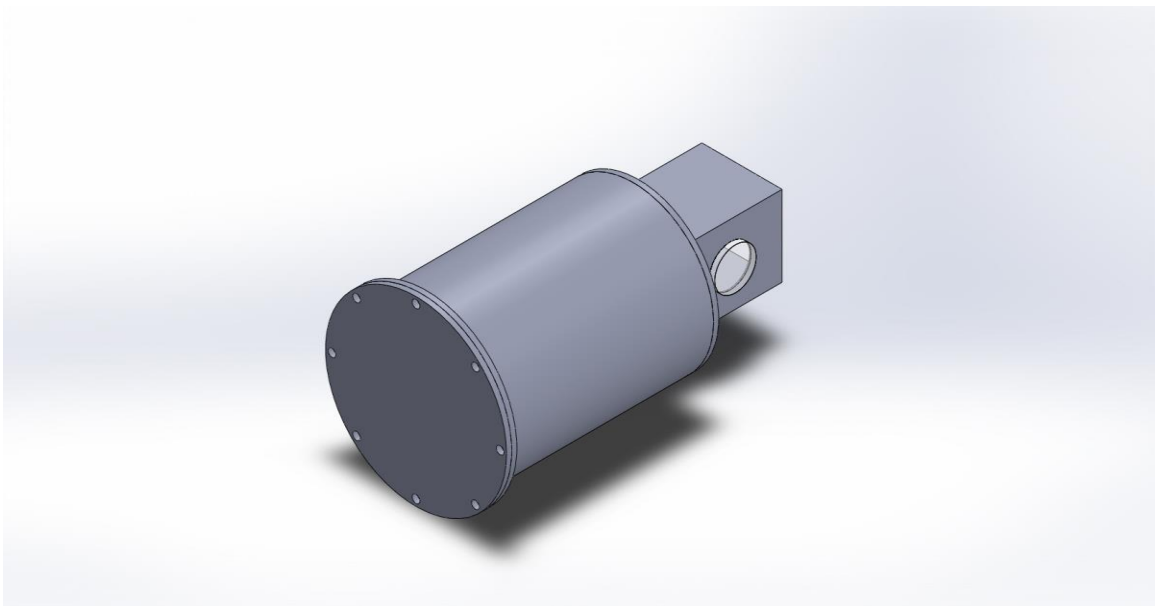


Figure 25 Isometric View of 3D Model Of Dump Tank and Test Section Assembly.

An acrylic sheet of 5mm thickness in the test section was used for fabricating the window. The window was of 80 mm diameter. Acrylic sheets have higher strength, stiffness and they are lighter compared to glass.

The test section was arc welded to inlet of the dump tank and the exit of the dump tank was enclosed with a 300mm flange as described in figure 25.

The dump tank was made from a 300 mm diameter MS tube, while a MS sheet was of 5mm thickness be used to fabricate the test section and the flange.

4.5 Calibration and Experimental Setup:

4.5.1 Calibration of the Shock tube:

An aluminum foil of 0.14mm was used to separate the driver and driven section. The end the driven section was closed with a solid flange. The shock tube was manually operated by pushing the piston. The obtained Mach number and pressure ratios were compared with the analytical values obtained through analytical calculations.

4.5.2 Calibration of the hypersonic wind tunnel:

After the calibration of the shock tube was successful. The convergent-divergent nozzle was attached at the end of the driven section. The driven section and the nozzle was separated with an aluminum foil of 0.07 mm (exactly half thickness of the diaphragm that separated the driver and the driven section). The shock tube was operated under the exact same condition. The exit Mach number obtained should be near the Mach number calculated analytically. KPJ Reddy (2015).

4.6 Schlieren Setup:

The schlieren single mirror setup with high-speed camera was used to capture the image of shockwave formed inside the shock tunnel. A mirror of focal length 40 mm and a diameter 75 mm was placed inside the test section. A LED light, which worked as a point light source was placed at a distance of $2F = 80$ mm from the mirror. A knife-edge was used to block the bright light. So, that the rays capturing the airflow was enhanced. A high-speed camera was placed behind the knife-edge as shown in figure 26. The frame rate was set to 5406.574 frames per second. The Resolution was 800X480. A MS plate of thickness 2mm, sustaining an angle of 24 degree was kept in the test section as the test object.



Figure 26 Schlieren Setup.

4.7 Experimental Setup:

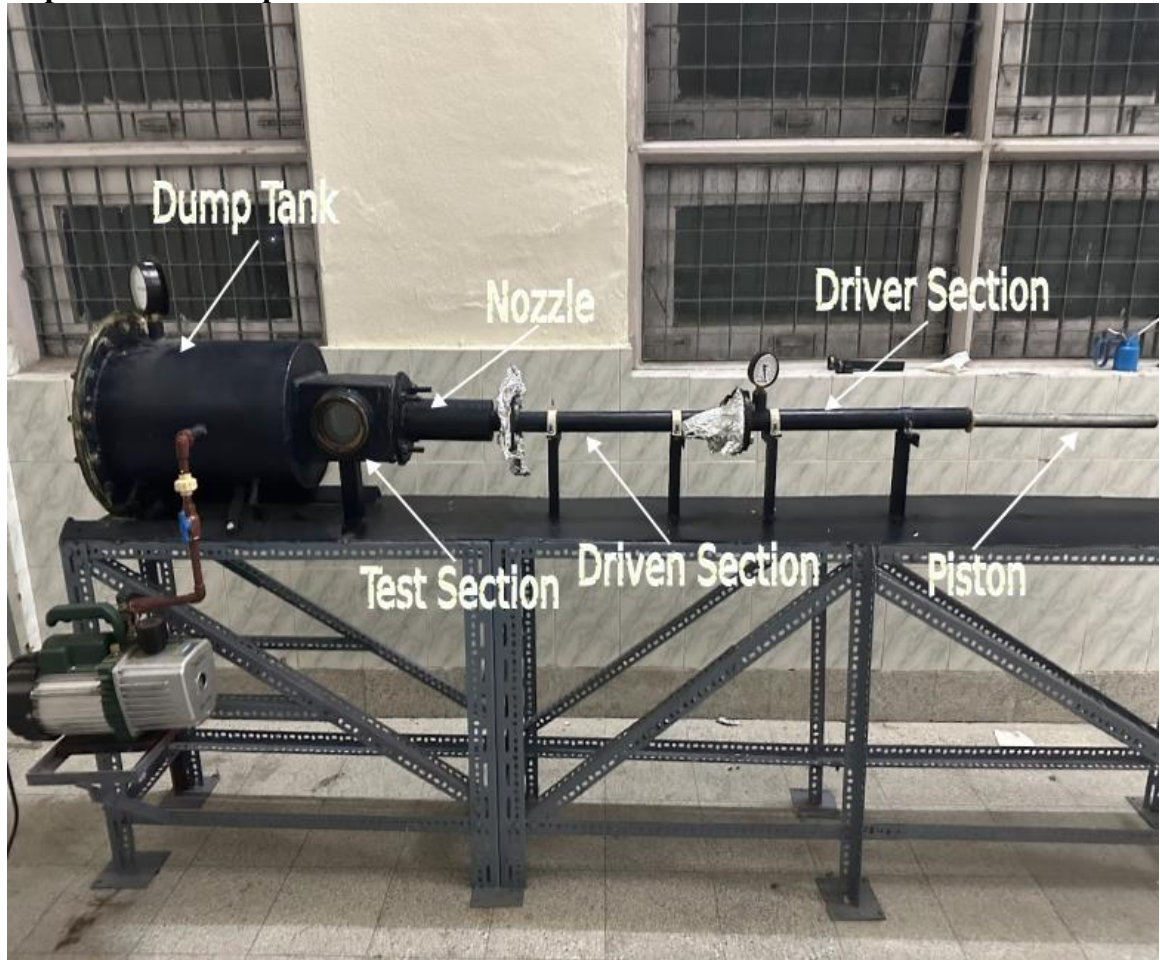


Figure 27 Final Experimental Setup.

Figure 27 shows the final experimental setup of the shock tunnel.

4.8 Case Setup for Simulation:

The CFD simulation were done in Open Foam, version 2112.

4.8.1 Shock tube:

1. Geometry:

The geometry of the shock tube was drawn in the design modeler of ANSYS student 2023. The length of the driver section was 490 mm and the length of driven section was 510 mm. The total length of shock tube was 1000mm and the diameter was 32mm. The scale of the model was 1:1 and a face split was done to separate the driver and driven section of shock tube.

2. Meshing:

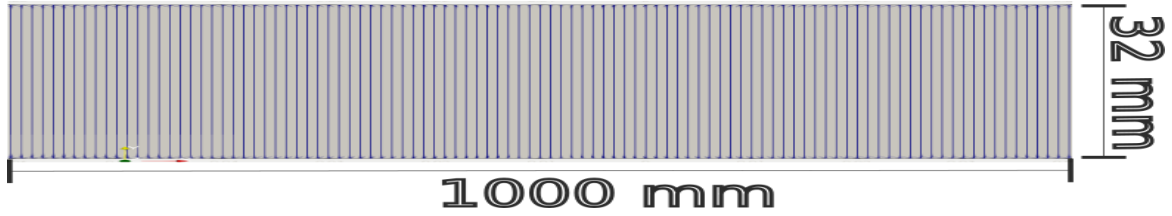


Figure 28 Domain Discretization of Shock tube

The tutorial case of shock tube available in OpenFoam was used to create the mesh. The number of elements were 1000. The shape of each cell was hexahedral and face meshing was done to achieve structured 1-Dimensional mesh as shown in figure 28.

3. Setup:

| S.N | Category | Parameters | Definition |
|-----|-----------|----------------------|-----------------|
| 1 | General | Flux scheme | Kurganov |
| | | ddt Scheme | Euler |
| | | Grad Scheme | Guass Linear |
| | | Interpolation Scheme | Linear, Vanleer |
| | | Courant Number | 0.2 |
| 2 | Modelling | Energy Equation | ON |
| | | Viscous Model | Inviscid |
| 3 | Material | Density | Ideal Gas |
| | | C_p | 1006.43 J/Kg.K |
| | | γ | 1.4 |
| | | Mean Molecular Mass | 28.966 g/mol |

Table 2 Solver Setup of Shock tube.

As the flow was compressible, the density based solver was used and the type of fluid used was inviscid. The energy equation was solved in this simulation. Air was used as the operating fluid and density relationship was set to follow ideal gas law. FV schemes were used in this simulation. The flux limiter Kurganov was used to limit the oscillations

(wiggles) that occur with higher order spatial discretization schemes due to shocks and sharp wave fronts. Euler time scheme (ddt scheme) was used and the max courant number was set to 0.2 to achieve stability in the simulation and reduce the numerical diffusion of Euler first order discretization scheme. The Guass linear is a second order, unbounded scheme. It uses Guassian integration, which is based on summing values on cell faces, which must be interpolated from cell centers. It is accurate but not robust; however, it is a recommended scheme. In the interpolation scheme, scalar field was set to Vanleer and the vector field was set to VanleerV. Vanleer uses a second order accuracy and it is composed of upwind and central differencing. Vanleer is a second order high-resolution shock-capturing scheme.

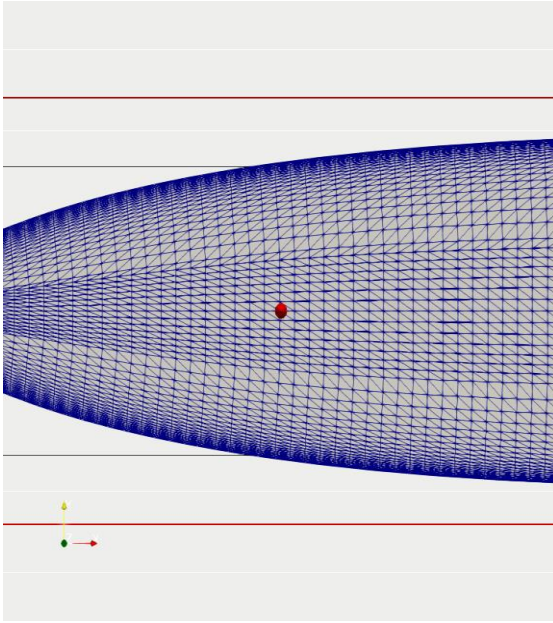
The pressure in the driver section was user-defined, 952000 Pa whereas the driven section was setup in atmospheric pressure i.e. 101325 Pa. The pressure boundary condition was set to zero gradient whereas; the walls was initially set to 101325 Pa. The temperature was set to zero gradient in the entry, exit and walls.

4.8.2 Nozzle:

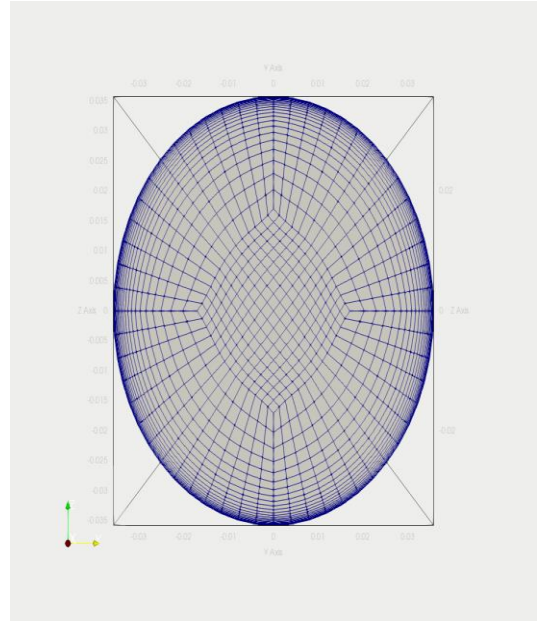
1. Geometry:

The Nozzle geometry was designed in MATLAB using MOC. Then, it was imported in a CAD software, which was later imported to ANSYS design modeler. The convergent and divergent part of nozzle were separated using the face split to achieve structured mesh.

2. Meshing:



(a)



(b)

Figure 29 (a) Domain Discretization of Nozzle and (b) Butterfly Grid of Nozzle.

The meshing of 3-D axisymmetric nozzle was done in Ansys Student 2023 R1. Automated meshing was done and then face meshing was used to obtain the structured mesh as shown in figure 29 (a). Inflation was used to obtain the butterfly grid. The butterfly grid in circular structure separates the circle into five different rectangular regions as shown in figure 29 (b). A central square is surrounded by four sided regions, which provides a good quality structured grid. The major advantage of butterfly grid in circular structure is that it can be handled by most of the solver when compared to H-grid, O-grid and unstructured grid.

The number of elements were 110544 and there were six faces per cells as it was three-dimensional mesh. The cell were hexahedral in shape.

3. Setup:

| S.N | Category | Parameteres | Defination |
|-----|-----------|------------------------------|-------------------|
| 1 | General | Flux Scheme | Kurganov |
| | | ddt Scheme | Backward |
| | | Gradient Scheme | Gauss Linear |
| | | Interpolation Scheme | Linear, vanAlbada |
| | | Courant Number | 0.1 |
| 2 | Modelling | Energy Equation | ON |
| | | Viscous model, time marching | No slip, laminar |
| 3 | Material | Density | Ideal Gas |
| | | C_p | 1006.43 J/Kg.K |
| | | γ | 1.4 |
| | | Mean Molecular Mass | 28.966 g/mol |

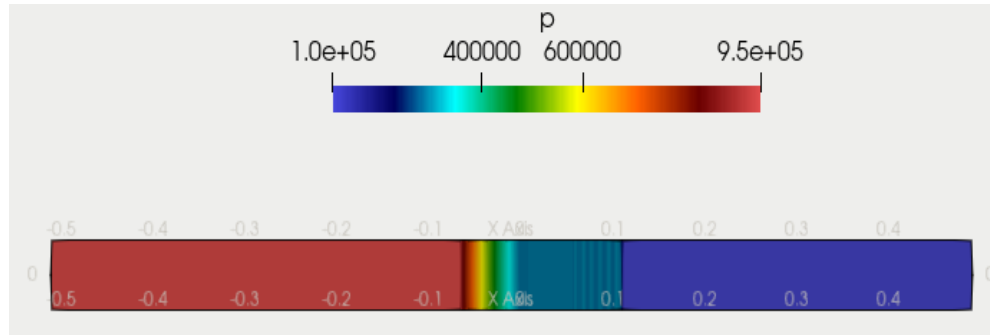
Table 3 Solver setup of Nozzle.

The ddt scheme used in the nozzle simulation was backward. This is a second order unbounded discretization scheme. It is more accurate compared to Euler first order scheme. The backward scheme helps to maintain an acceptable wave condition within the vicinity of the nozzle. As we do not need to bind the volume phase, we have not used Crank-Nicolson scheme. The courant number was set to 0.1 to minimize the oscillatory behavior of the backward second order scheme. The time marching was set to laminar and the fluid was set as viscous.

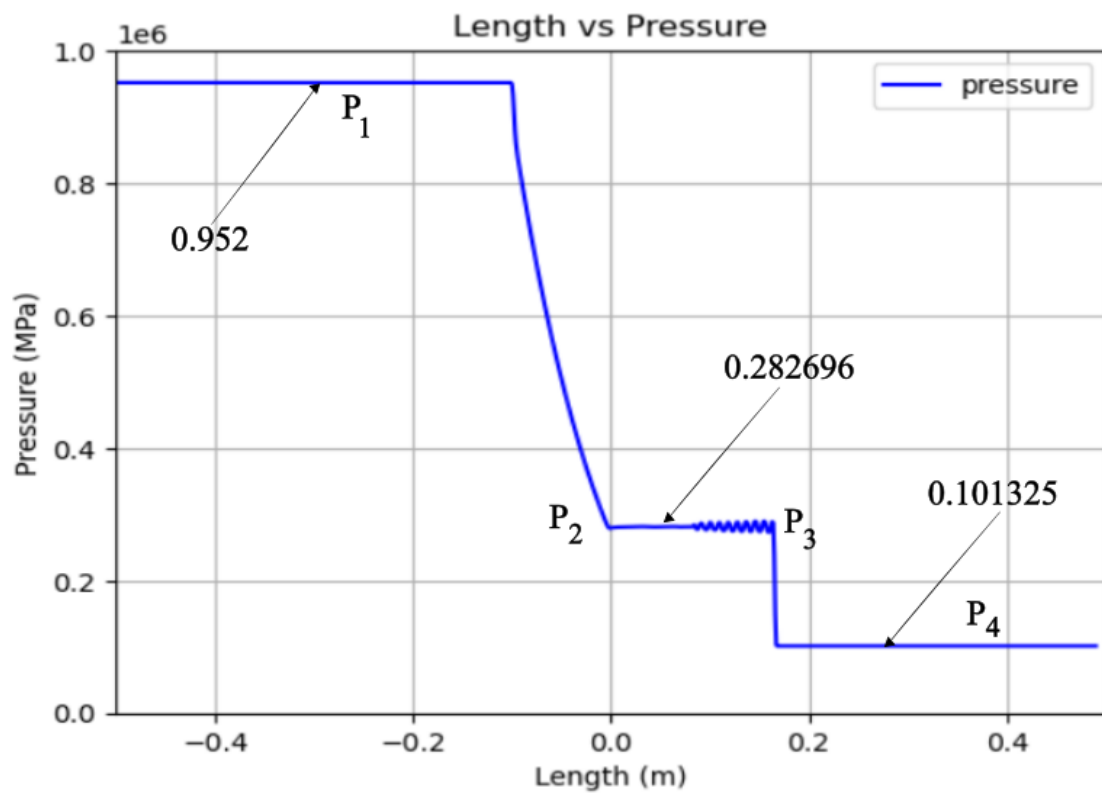
The inlet boundary condition type was total pressure and it was set to 764220 Pascal. The inlet pressure of the nozzle was set same as the exit pressure obtained from the driven section of the shock tube. The outlet boundary condition type was wave transmission and the initial value was set to 483.75 Pascal as obtained through analytical calculations. The inlet temperature was set to 432 kelvin, which was obtained at the exit of the shock tube and wall temperature was set to 300 kelvin. The velocity was set as zero gradient.

Chapter 5 Result and Discussion

5.1 Simulation Results of the Shock Tube:



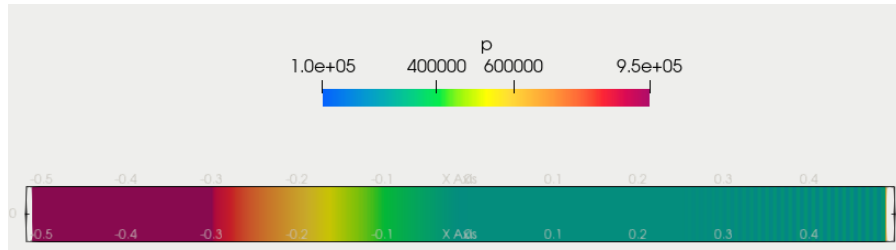
(a)



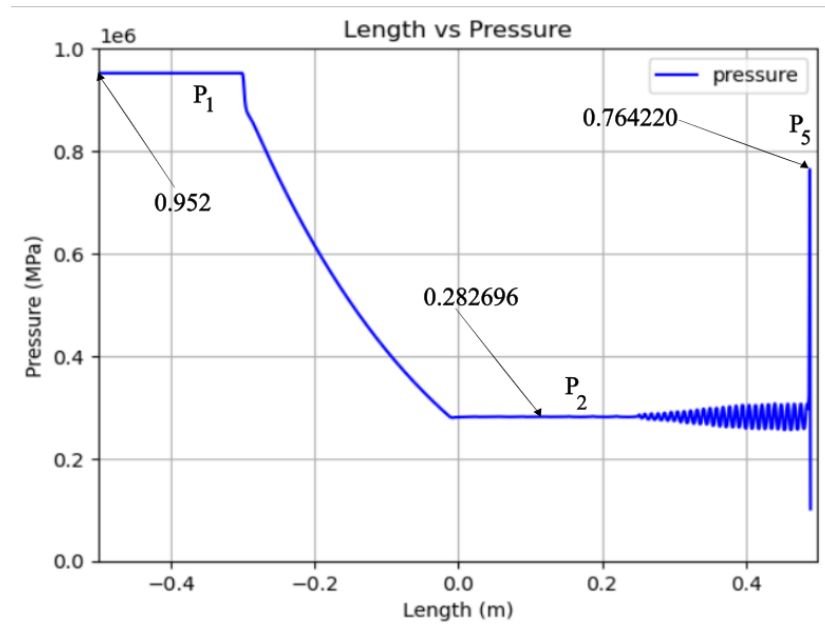
(b)

Figure 30 (a) static pressure contour and (b) static pressure plot of Shock tube after initial diaphragm burst

When the first diaphragm burst initially at a pressure of 952000 Pa, which was user-defined. The pressure in the driven section was initially set to 101325 Pa. The flow started to travel to the driven section. Hence, the pressure in the driven section beyond the shockwave started to increase as shown in figure 30 (a). The pressure plot in figure 30 (b) shows that the pressure P_4 in the driven section was 952000 Pa for the entire length. The pressure P_2 beyond the shockwave was 282696 Pa. Similarly, P_2 and P_3 have the same pressure as shockwave propagated to these region. The pressure P_1 was still atmospheric where the shock did not travelled.



(a)



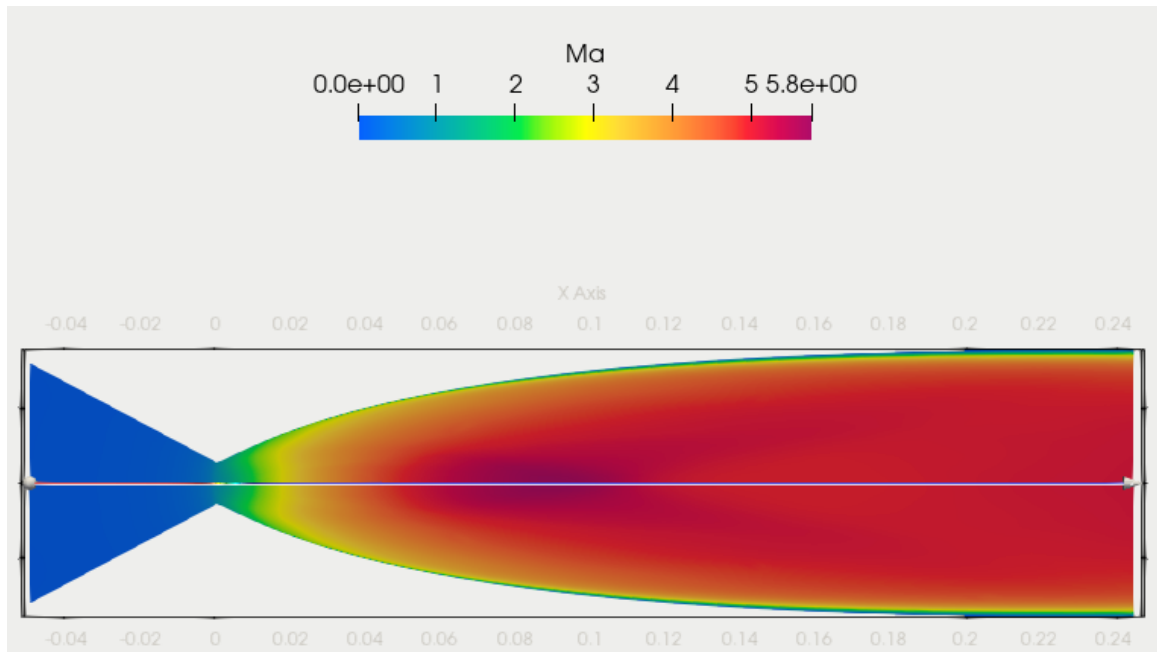
(b)

Figure 31 (a) Static pressure contour and (b) static pressure plot of Shock tube after deflection.

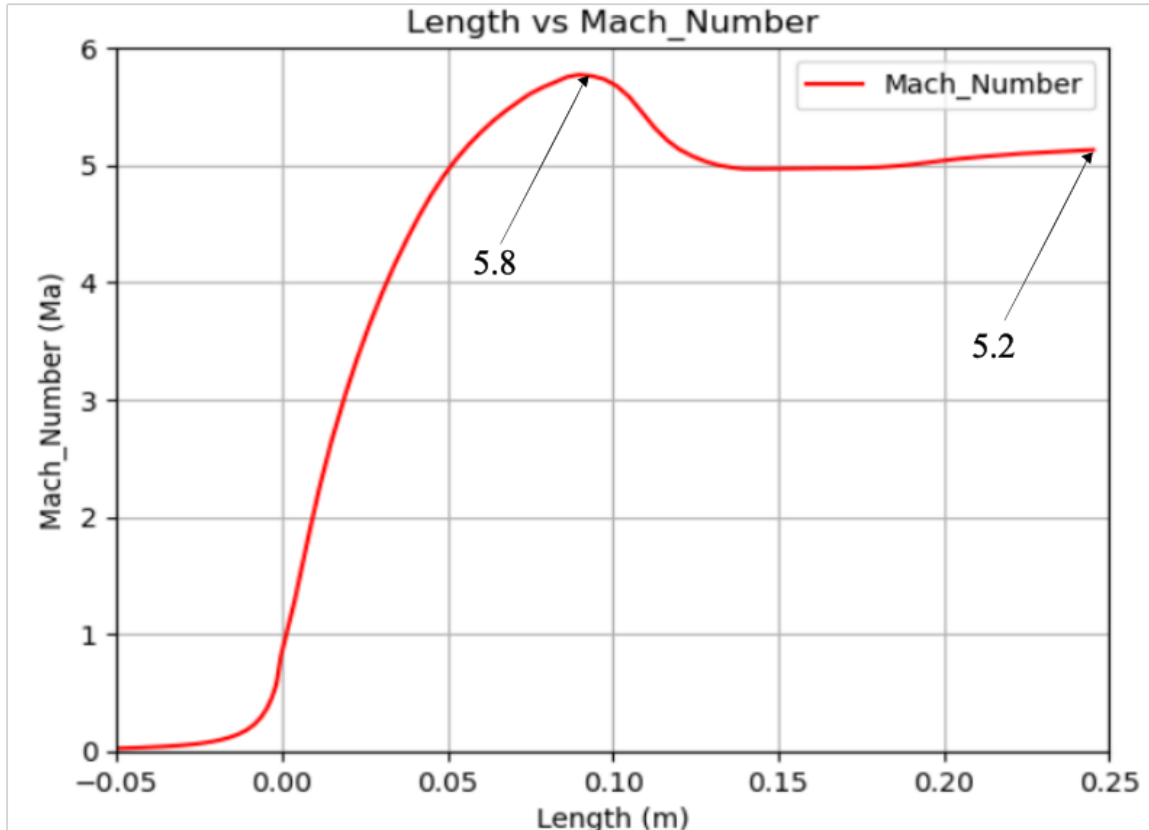
The pressure contour shown in figure 31 (a) is the shock propagation after the shockwave has hit the second diaphragm and pressure P_5 has increased to 764220 Pa. Which was used as the inlet pressure of the nozzle. It could be seen that the expansion fan has also started to travel in reverse direction of the shockwave towards the end of the driver section. The plot in figure 31 (b) shows that the length of driver section sustaining initial pressure of 952000 Pa has decreased from 510 mm to 230 mm as expansion fan has started towards the driver section. The oscillations were seen due to coarse mesh which could be decreased by increasing the grid points. The results obtained through these simulations were satisfactory for this project. Hence, further simulations were not done by increasing the elements.

5.2 Simulation Results of the Nozzle:

5.2.1 Mach Number in Nozzle:



(a)

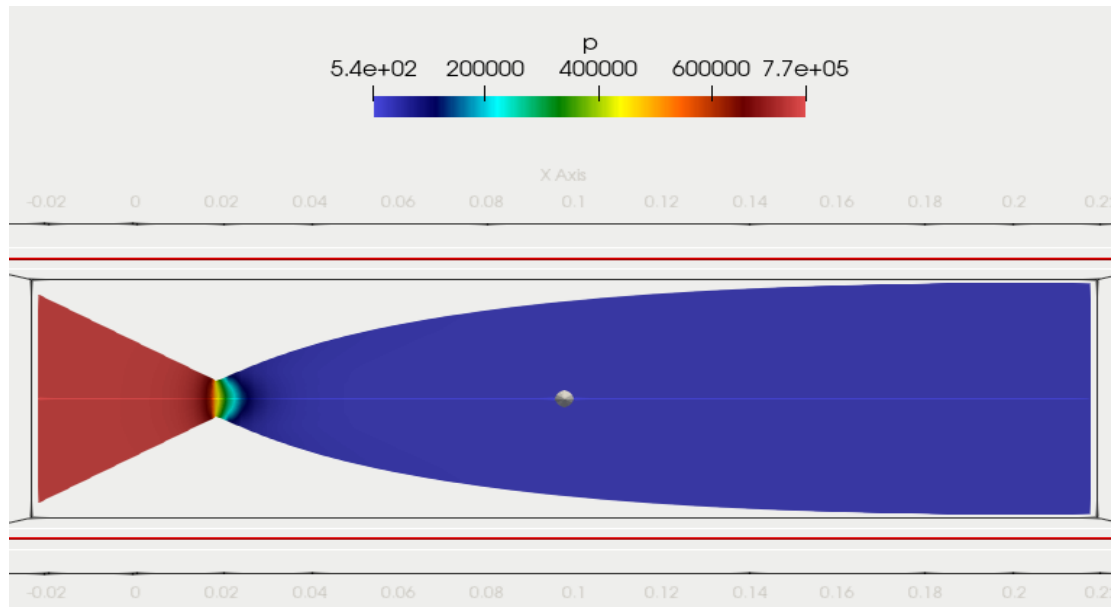


(b)

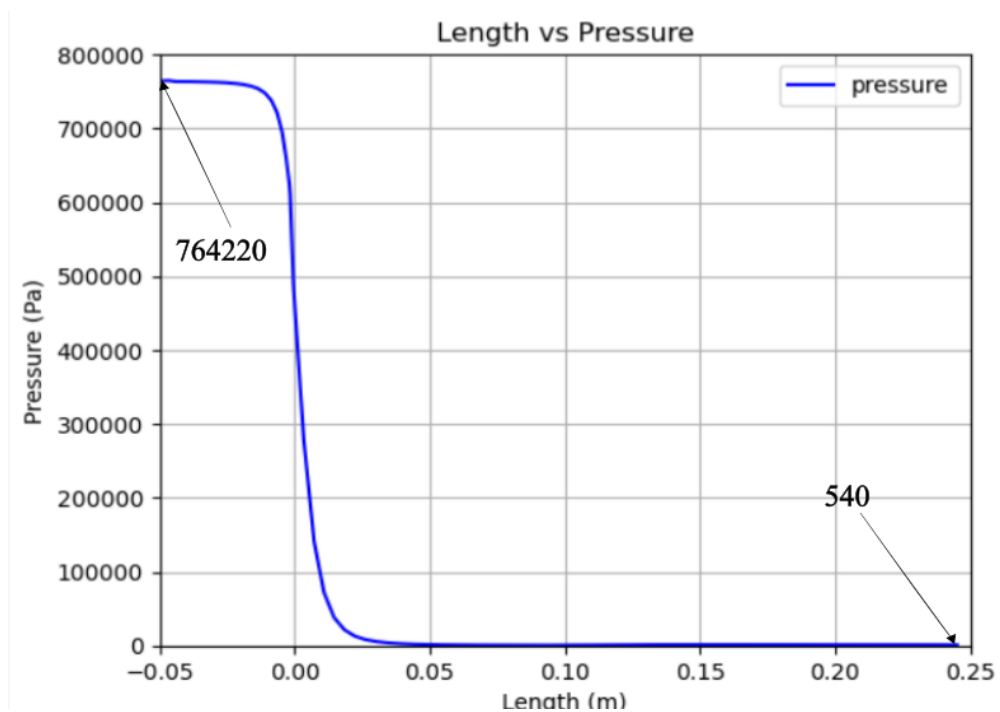
Figure 32 (a) Mach number contour and (b) Mach number plot of Nozzle.

The nozzle simulation (viscous and laminar) were done in OpenFoam v2112. As seen in figure 32(a). The convergent section was subsonic, choking occurred in the throat of the nozzle, and the diverging section expanded the air to hypersonic speed above Mach number 5. The pressure plot in figure 31(b) shows that at 140 mm, the Mach number was at peak 5.8, it decreased to Mach number 5 at 200mm and finally the Mach number is 5.2 at the exit. This happened because the nozzle was not perfectly expanded. Hence, the Matlab code could be improved to achieve a higher accuracy and better simulation results.

5.2.2 Static Pressure in Nozzle:



(a)



(b)

Figure 33 (a) Static pressure contour and (b) Static Pressure Plot of Nozzle.

The static pressure in the nozzle as shown in figure 33 (a). The convergent section has high pressure whereas, the pressure decreased rapidly as the velocity in the diverging section increased. The plot in figure 33 (b) shows that the stagnant pressure at the start of the converging section was 762000 KPa, which was user-defined. Hence, there was a sharp pressure decrease in pressure as the flow was induced. At the throat, the pressure was near atmospheric and further decreased below 50 Kpa as the air expanded in the diverging section and pressure was as low as 0.5 Kpa at the exit of the nozzle.

5.3 Experimental Result of Shock tube:

An experiment was conducted in the shock tube to verify the simulation results. A 0.14 mm thick aluminum foil was used as the initial diaphragm. The piston was pushed using human force and it showed that diaphragm was burst at a length of 100 mm from the end of the driver section. As the length of the driven section was 490 mm the X/L ratio was about 0.2.

| X/L | p_4/p_1 | p_2/p_1 | M_s |
|-----|-----------|-----------|-------|
| 0.1 | 25.12 | 4.05 | 1.90 |
| 0.2 | 9.52 | 2.79 | 1.59 |
| 0.3 | 5.40 | 2.20 | 1.42 |
| 0.4 | 3.61 | 1.84 | 1.31 |
| 0.5 | 2.64 | 1.64 | 1.23 |

Table 4 Estimated pressure values in the shock tube at different X/L ratios. (Reddy & Sharath, Manually Operated Piston Driven Shock Tube, 2013)

Inventor of manual piston driven shock tunnel KPJ Reddy provided information in table 4 estimated the isentropic pressure values at different X/L ratio. X represents the length ahead of the piston. Whereas, L represents the total length of the driver section. As mentioned, the initial diaphragm burst in this project was at $X/L = 0.2$. Which constitutes that the pressure for diaphragm burst was 9.52 Kpa and hence, the Mach number developed in the driven section was 1.59. The burst pattern was as anticipated as shown in figure 34.

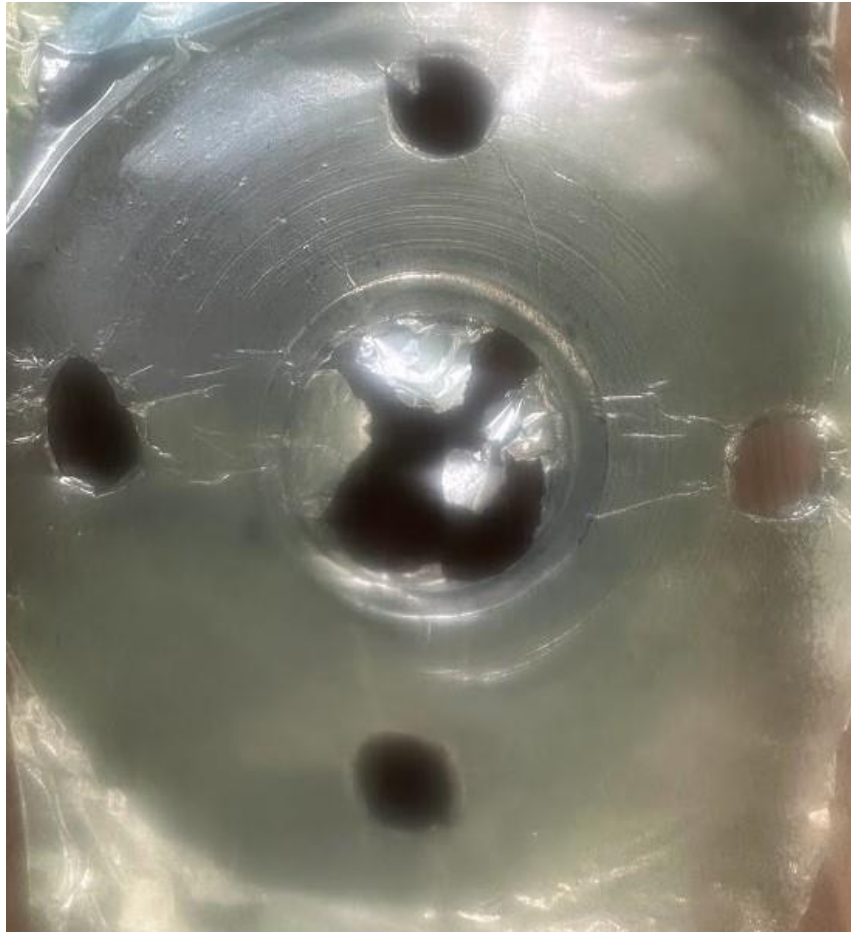


Figure 34 Initial Diaphragm burst of Shock tube.

5.4 Experimental Results of Nozzle and Shock formation:

A second diaphragm of 0.07mm was placed between the driven section and nozzle inlet. The similar process of shock tube operation was repeated but with the nozzle, test section and dump tank assembly. The pressure in the dump tank was reduced to 13332.2 Pascal using vacuum pump.



(a)



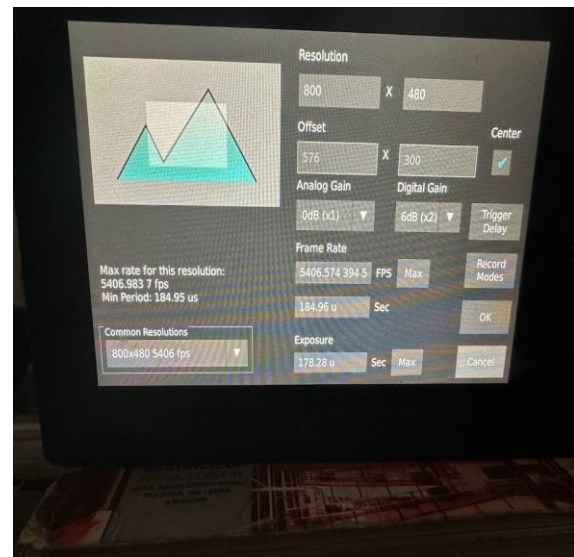
(b)

Figure 35 (a) and (b) Second diaphragm burst of Shock tube and Nozzle.

As shown in figure 35 (a) and 35 (b), the second diaphragm shows similar pattern of tear for different tests that were conducted. This demonstrated the consistency of the shock tunnel. A 2mm thick MS plate was bended to an angle of 24 degrees and it was welded in the test section as the test object to view the shock wave as shown in figure 36 (a). The frame rate in the Chronos high-speed camera was 5406.574 frame rates per second (FPS) and the resolution set to 840 X 480 mm as shown in figure 36 (b).



(a)



(b)

Figure 36 (a) and (b) Test object and high-speed camera setup for Schlieren Imaging.

An oblique shockwave and a bow shockwave were seen in the test section through schlieren setup as shown in figure 37 (a) and the tiff image was further processed in paraview 5.12.0-RC1 as shown in figure 37 (b).

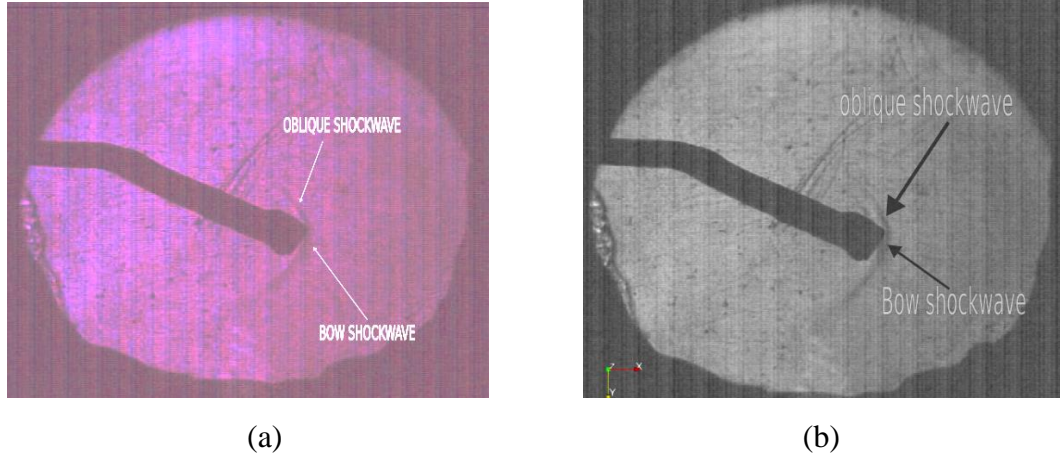
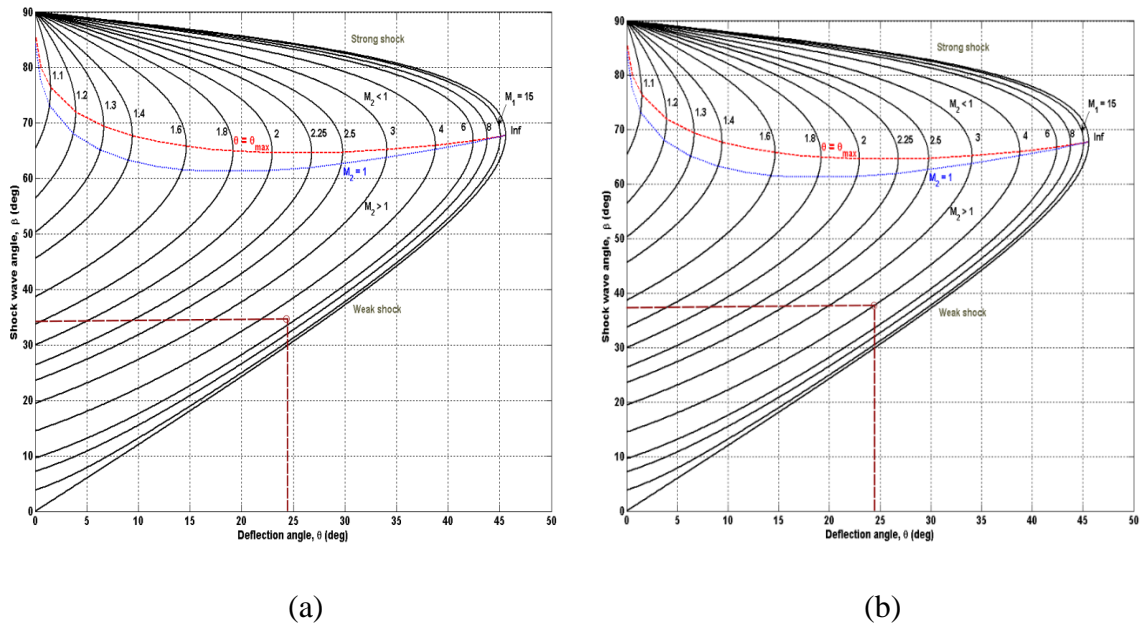
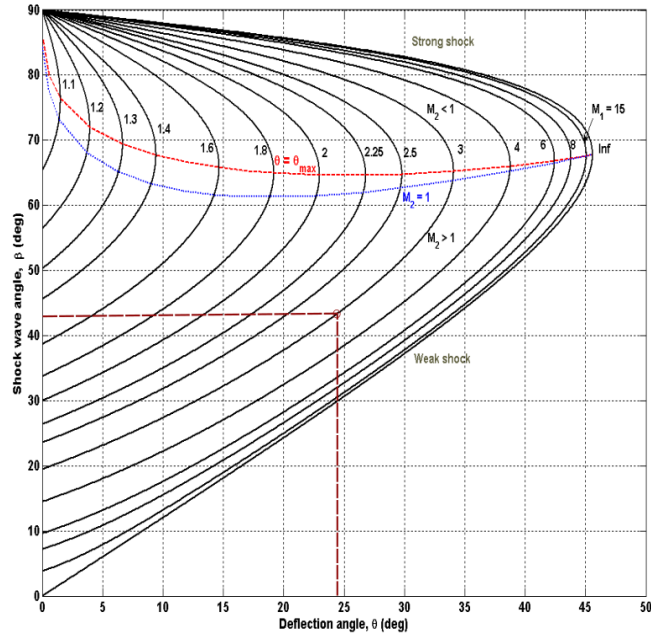


Figure 37 (a) and (b) Shockwave formation in Test Section.

The slope of the shock wave was measured using Matlab. It was found that ramp angle was 24 degrees and the wave angle varied from 32 degrees to 45 degrees. It was compared with the Theta-Beta-M plot. Which showed variation in Mach number 3 to 5 as shown in figure 38 (a), (b) and (c). Hence, concluding that shock tunnel operated near hypersonic boundaries.





(c)

Figure 38 Theth-Beta-M plot at (a) Ramp angle 24 degrees and wave angle 32 degree (b), Ramp angle 24 degree and wave angle 37 degrees and (c) Ramp angle 24 degrees and wave angle 45 degrees.

5.5 Budget:

| S.N. | DESCRIPTION | COST (NRS) |
|-------|--|------------|
| 1 | MS pipe and flanges 32 mm | 12,800 |
| 2 | Vacuum Pump | 50,000 |
| 3 | Acrylic | 3,000 |
| 4 | Dump tank and test section assembly | 20,000 |
| 5 | Manpower (WELDER, FITTER, etc) | 10,000 |
| 6 | Miscellaneous (Nuts Bolts, Mseal,Rubber Gasket, etc) | 10,000 |
| Total | | 1,05,800 |

Table 5 Final Budget of the project.

According to The Economic Times, India (2016), the cost of Reddy Tunnel was INR 6,00,000. Hence, this manual piston driven shock tunnel was moderately priced when compared to the Reddy tunnel but the quantifiable verification of Mach 6 could not be done

as procuring high frequency pressure transducer would further cost NPR 1,20,000. The inaccuracies in this shock tunnel could be further improved with time and minimal cost.

Chapter 6 Conclusion and Recommendation

6.1 Conclusion:

1. A manual piston driven shock tube was designed and fabricated using the local resources available in Nepal. The materials were procured locally and the shock tunnel was attached and installed here in Pulchowk Campus. The simulations and testing showed that the shock tunnel operated in atleast supersonic speeds.
2. The axisymmetric nozzle was designed using method of characteristics and they were simulated in OpenFoam v2112. The simulation results showed that the nozzle was working in hypersonic speeds. However, the simulation results showed that the expansion of the diverging section of nozzle was irregular. Hence, exit velocity ratio was Mach number 5.2. Even though this speed was in the hypersonic region, it was significantly less than the desired velocity of Mach number 5.8. The nozzle was machined in CNC lathe, but the manufactured nozzle had irregular surfaces, which might have affected nozzle speed in the experiments.
3. The verification of the shock tunnel was done using single mirror Schlieren technique and high-speed camera. An oblique shockwave and a bow shock was observed which verified that shock tunnel operated near hypersonic boundaries.
4. The initial diaphragm burst in the shock tube was at a pressure of 9.52 Kpa. This was verified using the estimated values of X/L ratio given by KPJ Reddy. The velocity ratio in the driven section was Mach number 1.59.
5. The total cost of designing and testing the manual piston driven shock tunnel was NRS 1,05,800, which was economical than Reddy Tunnel which costed INR 6,00,000.

6.2 Recommendations:

1. The axisymmetric nozzle that was designed using MOC, operated in hypersonic speeds (above Mach number 5), however the code and machining could be further improved to achieve higher accuracies.
2. In the future, procurement of high frequency transducers or manufacturing NPP pressure transducer could help to measure the exact speed in the test section of the shock tunnel.
3. An actuator or a hydraulic system could be used to push the piston, so the pressure at inlet of the nozzle could be set to a fixed value and the nozzle could be designed for a

particular net pressure ratio (NPR). Which would reduce the risk of over-expansion or under-expansion of the nozzle.

4. After improving this shock tunnel, a larger shock tunnel could be fabricated with proper funding.
5. High speed gases like helium, nitrogen, etc could be used as the driver gas to enhance the performance of the shock tube, which would result in achieving higher Mach number in driven section.
6. The driver gas could be preheated which would result in achieving higher Mach number number in the driven section.

References

1. Anderson, J. D. (2017). *Fundamentals of Aerodynamics*. New York: McGraw Hill Education.
2. Bertin, J. J. (1994). *Hypersonic Aerothermodynamics*. Washington: AIAA.
3. Braun, E. M., Lu, F. K., Panicker, P. K., Mitchell, R. R., Wilson, D. R., & Dutton, J. C. (2008). Supersonic Blowdown Wind Tunnel Control Using LabVIEW. *American Institute of Aeronautics and Astronautics*.
4. Bulat, P., Melnikova, A., Upyrev, V., & Volkov, K. (2021). Refraction of Oblique Shock Wave on a Tangential Discontinuity. *MPDI, Fluids*.
5. Gai, S. (1992). FREE PISTON SHOCK TUNNELS: DEVELOPMENTS AND CAPABILITIES. *Aerospace Science*.
6. HENDERSON, L. R. (2001). General Laws for Propagation of Shock Waves. *Handbook of Shock Waves*.
7. HORNUNG, H. G. (1988). 28th Lanchester Memorial Lecture —Experimental Real Gas Hypersonics. *Aeronautical Journal*.
8. Huang, P., Yonkers, S., Hokey, D., & Olenick, D. (2013). Screw pulsation generation and control: a shock tube mechanism. In I. o. Engineers, *8th International Conference on Compressors and their Systems* (pp. 113-128). London: Woodhead Publishing Limited.
9. J. Mee, D., Morgan, R., Paull, A., Jacobs, P., & Smart, M. K. (2017). The T4 Stalker Tube. *Springer International Publishing*.
10. Jiang, Z., Li, J., Hu, Z., Liu, Y., & Yu, H. (2020). On Theory and Methods for Advanced Detonation-Driven Hypervelocity Shock Tunnels. *National Science Publication*.
11. Khan, M. A., Sardiwal, S. K., Sharath, M., & Chowdary, D. (2013). Design of a Supersonic Nozzle using Method of Characteristics. *International Journal of Engineering Research & Technology*.

12. Kumar, C. S., & Reddy, K. P. (2015). Experiments in hand-operated, hypersonic shock tunnel facility. *Springer*.
13. Lynch, K. P., Spitzer, S., Grasser, T., Spillers, R., Farias, P., & Wagner, J. L. (2019). A Free-Piston Driven Shock Tube for Generating Extreme Aerodynamic Conditions: Design and First Shots. *AIAA Scitech*.
14. Morajkar, R. R., Klomparens, R. L., Eagle, W. E., Driscoll, J. F., Gamba, M., & Benek, J. A. (2015). Relationship Between Intermittent Separation and Vortex Structure in a Three-Dimensional Shock/Boundary-Layer Interaction. *AIAA*.
15. Moura, A. F., & Rosa, M. A. (2013). A COMPUTER PROGRAM FOR CALCULATING NORMAL AND OBLIQUE SHOCK WAVES FOR AIRFLOWS IN CHEMICAL AND THERMODYNAMIC EQUILIBRIUM. *22nd International Congress of Mechanical Engineering* (p. 11). Ribeirão Preto, SP: ABCM.
16. Ranabhat, S., Darlami, K., Bhattarai, S., & Shrestha, N. (2022). Numerical and Experimental Investigation of Exhaust Flow from Convergent-Divergent Nozzle. *IOE Graduate Conference*.
17. Reddy, K. (2007). Hypersonic Flight and Ground Testing Activities in India. *16th Australasian Fluid Mechanics Conference* (p. 7). Gold Coast: K.P.J Reddy IISC .
18. Reddy, K., & Sharath, N. (2013). Manually Operated Piston Driven Shock Tube. *Current Science*.
19. Rose, B. R., Jinu, G. R., & Brindha, C. J. (2015). A numerical optimization of high altitude testing facility for wind tunnel experiments. *Chinese Journal of Aeronautics* , 636-648.
20. Sudarshan, B., Pranav, H. A., & Sanjay, A. V. (2023). Hypersonic flow study in a pneumatically operated academic shock tunnel. *AIP Publishing*.
21. Tsien, H.-S. (1946). Similarity Laws of Hypersonic Flows. *Journal Of Mathematics and Physics*.

22. Vivek, P., & T.G.Sitharam. (2019). *Granular Materials Under Shock and Blast Loading*. Bangalore: Springer.

APPENDIX I

<https://www.mathworks.com/matlabcentral/fileexchange/85253-axisymmetric-minimum-length-nozzle-design-tool>

The base code was taken from the above link and modified for this project.

AxSymMLN.m

```
%% INPUT
```

```
mach_exit=6;
```

```
gamma=1.4;
```

```
N_lin=20; %linear kernel
```

```
N_comp=15; %compressed kernel - set 1 for uncompressed kernel
```

```
index_comp=5; %compression exponent
```

```
plot_text=false;
```

```
th=1e-7; %tolerance
```

```
AR=1; %aspect ratio for the transition region
```

```
%gamma=1.4;
```

```
%th=1e-7;
```

```
%% OUTPUT VALUES
```

```
theta_wmax=prandtl_meyer(mach_exit,gamma)/4; %AXSYM flows
```

```
delta_theta=theta_wmax/N_lin; %linear kernel
```

```
steps=N_lin+N_comp-1;
```

```
%number of points - KERNEL REGION
```

```
n_kernel=0;
```

```
for i=0:steps
```

```
    n_kernel=n_kernel+steps-i;
```

```
end
```

```
kernel=zeros(n_kernel,4);
```

```
sel=@(x) steps+1+x.*(steps-0.5*(x+1)); %new series
```

```
figure(1)
```

```

grid
daspect([1 1 0.2778])
hold on

%% KERNEL REGION
% Compute points on the first characteristic line (origin)
% Compression region
% Compute point 1 - 3RD UNIT PROCESS
theta1=(1/N_comp).^index_comp*delta_theta; %theta
mach1=fsolve(@(x) prandtl_meyer(x,gamma)-theta1,1.1,options); %mach
r1=1; %ORIGIN
x1=0; %ORIGIN
kernel(1,:)=unit_process3([theta1,mach1,x1,r1]);
line([x1 kernel(1,3)], [r1 kernel(1,4)])
% Compute point 2 - 2ND UNIT PROCESS
if(N_comp>=2)
    theta1=(2/N_comp).^index_comp*delta_theta;
    mach1=fsolve(@(x) prandtl_meyer(x,gamma)-theta1,1.1,options); %mach
    r1=1; %ORIGIN
    x1=0; %ORIGIN
    kernel(2,:)=unit_process2([theta1,mach1,x1,r1],kernel(1,:));
    line([x1 kernel(2,3)], [r1 kernel(2,4)])
end
% Compute internal kernel points - 1ST UNIT PROCESS
for i=3:N_comp
    theta1=(i/N_comp).^index_comp*delta_theta;
    mach1=fsolve(@(x) prandtl_meyer(x,gamma)-theta1,1.1,options); %mach
    r1=1; %ORIGIN
    x1=0; %ORIGIN
    kernel(i,:)=unit_process1([theta1,mach1,x1,r1],kernel(i-1,:));
    line([x1 kernel(i,3)], [r1 kernel(i,4)])
end

```

```

end
% Linear region
if(N_comp>=2)
    for i=2:N_lin
        theta1=i*delta_theta;
        mach1=fsolve(@(x) prandtl_meyer(x,gamma)-theta1,1.1,options); %mach
        r1=1; %ORIGIN
        x1=0; %ORIGIN
        kernel(N_comp+i-1,:)=unit_process1([theta1,mach1,x1,r1],kernel(N_comp+i-2,:));
        line([x1 kernel(N_comp+i-1,3)],[r1 kernel(N_comp+i-1,4)])
    end
else
    i=2; % run unit process 2
    theta1=i*delta_theta;
    mach1=fsolve(@(x) prandtl_meyer(x,gamma)-theta1,1.1,options); %mach
    r1=1; %ORIGIN
    x1=0; %ORIGIN
    kernel(N_comp+i-1,:)=unit_process2([theta1,mach1,x1,r1],kernel(N_comp+i-2,:));
    line([x1 kernel(N_comp+i-1,3)],[r1 kernel(N_comp+i-1,4)])
    for i=3:N_lin
        theta1=i*delta_theta;
        mach1=fsolve(@(x) prandtl_meyer(x,gamma)-theta1,1.1,options); %mach
        r1=1; %ORIGIN
        x1=0; %ORIGIN
        kernel(N_comp+i-1,:)=unit_process1([theta1,mach1,x1,r1],kernel(N_comp+i-2,:));
        line([x1 kernel(N_comp+i-1,3)],[r1 kernel(N_comp+i-1,4)])
    end
end
end
% Compute the remaining characteristics
% Compression region
for j=0:N_comp-1

```



```

%Centerline - 3rd unit process
kernel(sel(j),:)=unit_process3(kernel(sel(j-1)+1,:));
%line([kernel(sel(j-1),3) kernel(sel(j-1)+1,3)], [kernel(sel(j-1),4) kernel(sel(j-1)+1,4)])
line([kernel(sel(j-1),3) kernel(sel(j-1)+1,3)], [kernel(sel(j-1),4) kernel(sel(j-1)+1,4)])
line([kernel(sel(j-1)+1,3) kernel(sel(j),3)], [kernel(sel(j-1)+1,4) kernel(sel(j),4)])
%Adjacent - 2nd unit process
for i=1:N_comp-j-1
    kernel(sel(j)+1,:)=unit_process2(kernel(sel(j-1)+2,:),kernel(sel(j),:));
    line([kernel(sel(j-1)+2,3) kernel(sel(j)+1,3)], [kernel(sel(j-1)+2,4) kernel(sel(j)+1,4)])
    line([kernel(sel(j-1)+1,3) kernel(sel(j-1)+2,3)], [kernel(sel(j-1)+1,4) kernel(sel(j-1)+2,4)])
end
%Internal kernel points - 1st unit process
for i=2:N_comp-j-1
    kernel(sel(j)+i,:)=unit_process1(kernel(sel(j-1)+i+1,:),kernel(sel(j)+i-1,:));
    line([kernel(sel(j-1)+i,3) kernel(sel(j-1)+i+1,3)], [kernel(sel(j-1)+i,4) kernel(sel(j-1)+i+1,4)])
    line([kernel(sel(j-1)+i+1,3) kernel(sel(j)+i,3)], [kernel(sel(j-1)+i+1,4) kernel(sel(j)+i,4)])
end
end
% Linear region
for j=0:steps-2
    if(j<=N_comp)
        ind_ext=sel(j)+N_comp-j;
    else
        ind_ext=sel(j);
    end
    for i=ind_ext:sel(j+1)-1
        k=i+1-sel(j);
        switch k

```

```

case 1
    %UNIT PROCESS 3
    kernel(sel(j,:)=unit_process3(kernel(sel(j-1)+1,:));
    line([kernel(sel(j-1),3)    kernel(sel(j-1)+1,3)], [kernel(sel(j-1),4)    kernel(sel(j-1)+1,4)])
    line([kernel(sel(j),3) kernel(sel(j-1)+1,3)], [kernel(sel(j),4) kernel(sel(j-1)+1,4)])
case 2
    %UNIT PROCESS 2
    kernel(sel(j)+1,:)=unit_process2(kernel(sel(j-1)+2,:),kernel(sel(j),:));
    line([kernel(sel(j-1)+1,3) kernel(sel(j-1)+2,3)], [kernel(sel(j-1)+1,4) kernel(sel(j-1)+2,4)])
    line([kernel(sel(j-1)+2,3)    kernel(sel(j)+1,3)], [kernel(sel(j-1)+2,4)
kernel(sel(j)+1,4)])
otherwise
    %UNIT PROCESS 1
    ind_inn=sel(j-1)+(i-sel(j)+1);
    kernel(i,:)=unit_process1(kernel(ind_inn,:),kernel(i-1,:));
    line([kernel(ind_inn-1,3)    kernel(ind_inn,3)], [kernel(ind_inn-1,4)
kernel(ind_inn,4)])
    line([kernel(ind_inn,3) kernel(i,3)], [kernel(ind_inn,4) kernel(i,4)])
end
end
end

%% TRANSITION REGION
transition=zeros(2*steps*(steps+1),4);
XY=zeros(2*steps+1,2);
% Compute mean distance on the last right-running characteristic
S_ave=mean(sqrt(diff(kernel(sel(0:steps-1)-1,3)).^2+diff(kernel(sel(0:steps-1)-1,4)).^2));
S_plus=AR*S_ave;
mu_exit=asin(1/kernel(end,2));

```

```

%x_exit=sqrt(area_mach_nozzle(mach_exit,gamma))/tan(mu_exit)+kernel(end,3);

% Compute first transition point
transition(1,2)=kernel(end,2);
transition(1,3)=S_plus*cos(mu_exit)+kernel(end,3);
transition(1,4)=S_plus*sin(mu_exit)+kernel(end,4);
line([kernel(end,3) transition(1,3)],[kernel(end,4) transition(1,4)],'Color','black')
% Compute first transition line
for j=steps-2:-1:0
    transition(steps-j,:)=unit_process1(transition(steps-j-1,:),kernel(sel(j)-1,:));
    line([transition(steps-j,3) transition(steps-j-1,3)],[transition(steps-j,4) transition(steps-j-1,4)],'Color','black')
    line([transition(steps-j,3)    kernel(sel(j)-1,3)],[transition(steps-j,4)    kernel(sel(j)-1,4)],'Color','black')
end
transition(steps-j+1,:)=unit_process1(transition(steps-j,:),[transition(steps-j,1)
transition(steps-j,2) 0 1]);
line([transition(steps-j+1,3) transition(steps-j,3)],[transition(steps-j+1,4) transition(steps-j,4)],'Color','black')
line([0 transition(steps-j+1,3)],[1 transition(steps-j+1,4)],'Color','black')

% Compute initial contour slope (theta_wmax)
m_lim=(transition(steps,4)-1)/transition(steps,3);
NEXT=false;
cc=steps; %identify column on the transition web
bb=0; %identify row on the transition web
XY(1,:)= [0 1]; %initial contour point (throat region)
k=2; %contour counter
while(NEXT==false)
    if(tan(theta_wmax)>m_lim)
        %fprintf('Intersects C- %d\n',k)

```

```

NEXT=true;
point_new=wall_minus(theta_wmax,XY(k-
1,:),transition(bb*(steps+1)+cc,:),transition(bb*(steps+1)+cc+1,:)); %theta,r,x
XY(k,:)=[point_new(3),point_new(2)]; %SAVE CONTOUR POINT
line([0 XY(k,1)],[1 XY(k,2)],'Color','black','LineWidth',4)
k=k+1;
bb=bb+1;
else
    %fprintf('Intersects C+ %d\n',k)
    NEXT=false;
    point_new=wall_plus(theta_wmax,XY(k-1,:),transition((bb-
1)*(steps+1)+cc,:),transition(bb*(steps+1)+cc+1,:)); %theta,r,x
    XY(k,:)=[point_new(3),point_new(2)]; %SAVE CONTOUR POINT
    line([0 XY(k,1)],[1 XY(k,2)],'Color','black','LineWidth',4)
    k=k+1;
    cc=cc-1;
end
end

i=0;
OUTLET=false;
while(OUTLET==false)
    i=i+1;
    transition(i*(steps+1)+1,2)=kernel(end,2);
    transition(i*(steps+1)+1,3)=S_plus*cos(mu_exit)+transition((i-1)*(steps+1)+1,3);
    transition(i*(steps+1)+1,4)=S_plus*sin(mu_exit)+transition((i-1)*(steps+1)+1,4);
    line([transition(i*(steps+1)+1,3) transition((i-
1)*(steps+1)+1,3)],[transition(i*(steps+1)+1,4) transition((i-
1)*(steps+1)+1,4)],'Color','black')
    for j=steps-2:-1:-1+(steps-cc)

```

```

        transition(i*(steps+1)+steps-j,:)=unit_process1(transition(i*(steps+1)+steps-j-
1,:),transition((i-1)*(steps+1)+steps-j,:));
        line([transition(i*(steps+1)+steps-j,3)                transition(i*(steps+1)+steps-j-
1,3)],[transition(i*(steps+1)+steps-j,4) transition(i*(steps+1)+steps-j-1,4)],'Color','black')
        line([transition(i*(steps+1)+steps-j,3)                transition((i-1)*(steps+1)+steps-
j,3)],[transition(i*(steps+1)+steps-j,4)                transition((i-1)*(steps+1)+steps-
j,4)],'Color','black')
    end

    NEXT=false;
    while(NEXT==false && OUTLET==false)
        theta0=point_new(1);
        m_lim=(transition(bb*(steps+1)+cc,4)-XY(k-1,2))/(transition(bb*(steps+1)+cc,3)-
XY(k-1,1)); %constant
        point_new=wall_contour(m_lim,theta0,XY(k-1,:),...
        transition((bb-
1)*(steps+1)+cc,:),transition(bb*(steps+1)+cc,:),transition(bb*(steps+1)+cc+1,:));
        XY(k,:)=[point_new(3),point_new(2)]; %SAVE CONTOUR POINT
        line([XY(k-1,1) XY(k,1)],[XY(k-1,2) XY(k,2)],'Color','black','LineWidth',4)
        k=k+1;
        if(NEXT)
            bb=bb+1;
        else
            cc=cc-1;
            if(cc<=0)
                OUTLET=true;
            end
        end
    end
end
end
end
title('Axisymmetric minimum-length nozzle contour','FontSize',20,'FontWeight','bold')

```

```

xlabel('x/r_{throat}','FontSize',16,'FontWeight','bold')
ylabel('y/r_{throat}','FontSize',16,'FontWeight','bold')

%% EXPORT
export=zeros(size(XY,1),3);
export(:,1)=1;
export(:,2:3)=XY(:,,:);

format short
writematrix(export,'nozzle_axi.txt','Delimiter','tab')

end

```

Point for Nozzle Contour

| | | | | | |
|---------|---------|---------|---------|---------|---------|
| 0 | 5.5 | 9.29204 | 9.77172 | 30.2314 | 17.5035 |
| 0.03497 | 5.51593 | 9.98704 | 10.0854 | 31.3804 | 17.8331 |
| 0.18566 | 5.58674 | 10.5137 | 10.3205 | 32.5105 | 18.1623 |
| 0.40983 | 5.68072 | 10.7208 | 10.4115 | 33.6235 | 18.4913 |
| 0.68525 | 5.79772 | 11.4738 | 10.741 | 34.7207 | 18.8199 |
| 1.00682 | 5.9358 | 11.882 | 10.919 | 34.9288 | 18.8798 |
| 1.37058 | 6.09338 | 12.2422 | 11.073 | 35.9187 | 19.1414 |
| 1.77317 | 6.269 | 13.0281 | 11.4074 | 37.1661 | 19.4607 |
| 2.2116 | 6.4613 | 13.4462 | 11.5844 | 38.3927 | 19.7797 |
| 2.33987 | 6.51913 | 13.8316 | 11.7437 | 39.6005 | 20.0987 |
| 2.44987 | 6.57005 | 14.6553 | 12.0816 | 40.791 | 20.4174 |
| 2.67252 | 6.6735 | 15.2802 | 12.3365 | 41.2088 | 20.5252 |
| 2.90345 | 6.78129 | 15.4928 | 12.4209 | 42.0699 | 20.7288 |
| 3.16162 | 6.90227 | 16.3559 | 12.7611 | 43.4134 | 21.0355 |
| 3.62286 | 7.1194 | 17.124 | 13.0626 | 44.7347 | 21.3423 |
| 3.67629 | 7.14459 | 17.2314 | 13.1022 | 46.0358 | 21.6492 |
| 4.21669 | 7.4 | 18.2017 | 13.4433 | 47.3184 | 21.9561 |
| 4.5259 | 7.54665 | 19.1564 | 13.7846 | 48.1223 | 22.1415 |
| 4.77863 | 7.66639 | 20.0968 | 14.1258 | 48.6717 | 22.2571 |
| 5.32747 | 7.92632 | 21.0242 | 14.4669 | 50.1141 | 22.5492 |
| 5.3627 | 7.94295 | 21.9394 | 14.808 | 51.533 | 22.8416 |
| 5.96846 | 8.22899 | 22.8434 | 15.1489 | 52.9305 | 23.1344 |
| 6.21209 | 8.34417 | 23.3656 | 15.3371 | 54.3084 | 23.4275 |
| 6.59246 | 8.52302 | 23.8294 | 15.489 | 55.5651 | 23.6854 |
| 7.16083 | 8.78908 | 24.8969 | 15.8266 | 55.7355 | 23.7171 |
| 7.23633 | 8.82414 | 25.9464 | 16.1638 | 57.2806 | 23.9923 |
| 7.89997 | 9.13188 | 26.9796 | 16.5007 | 58.801 | 24.2683 |
| 8.17902 | 9.26122 | 27.9979 | 16.8373 | 60.2988 | 24.545 |
| 8.57978 | 9.44509 | 28.9219 | 17.1326 | 61.7757 | 24.8224 |
| 9.273 | 9.76301 | 29.0617 | 17.1735 | 63.2334 | 25.1003 |

| | | | | | |
|---------|---------|---------|---------|---------|---------|
| 63.8555 | 25.2139 | 108.637 | 30.9699 | 166.682 | 34.4916 |
| 64.7848 | 25.3668 | 110.682 | 31.1347 | 168.944 | 34.5874 |
| 66.4168 | 25.6239 | 112.703 | 31.302 | 171.189 | 34.6856 |
| 68.0245 | 25.8821 | 114.701 | 31.4716 | 171.266 | 34.6885 |
| 69.6099 | 26.1413 | 116.678 | 31.6433 | 173.581 | 34.7514 |
| 71.1747 | 26.4014 | 118.636 | 31.8169 | 176.03 | 34.8076 |
| 72.7204 | 26.6623 | 120.574 | 31.9925 | 178.461 | 34.8668 |
| 73.0074 | 26.7085 | 120.939 | 32.023 | 180.872 | 34.9287 |
| 74.3846 | 26.9064 | 122.65 | 32.1423 | 183.266 | 34.9933 |
| 76.1125 | 27.1433 | 124.802 | 32.2801 | 185.643 | 35.0604 |
| 77.8161 | 27.3817 | 126.931 | 32.4207 | 188.005 | 35.1299 |
| 79.4975 | 27.6214 | 129.037 | 32.5637 | 190.35 | 35.2018 |
| 81.158 | 27.8623 | 131.123 | 32.7092 | 190.568 | 35.2074 |
| 82.7993 | 28.1044 | 133.19 | 32.8568 | 192.825 | 35.2443 |
| 83.2214 | 28.1634 | 135.237 | 33.0066 | 195.355 | 35.2767 |
| 84.5586 | 28.3285 | 136.273 | 33.076 | 197.868 | 35.3119 |
| 86.3914 | 28.5431 | 137.393 | 33.1363 | 200.365 | 35.3497 |
| 88.1998 | 28.7595 | 139.658 | 33.2455 | 202.846 | 35.39 |
| 89.9856 | 28.9775 | 141.9 | 33.3576 | 205.312 | 35.4328 |
| 91.7502 | 29.1971 | 144.12 | 33.4725 | 207.764 | 35.4778 |
| 93.4952 | 29.4181 | 146.319 | 33.59 | 210.201 | 35.5251 |
| 94.4908 | 29.5373 | 148.499 | 33.71 | 210.338 | 35.5272 |
| 95.3337 | 29.6251 | 150.661 | 33.8323 | 212.75 | 35.5464 |
| 97.2797 | 29.8149 | 152.805 | 33.9567 | 215.338 | 35.5604 |
| 99.2008 | 30.0069 | 153.053 | 33.9697 | 217.913 | 35.5768 |
| 101.099 | 30.201 | 155.094 | 34.0509 | 220.474 | 35.5955 |
| 102.975 | 30.3969 | 157.452 | 34.1334 | 223.022 | 35.6163 |
| 104.831 | 30.5946 | 159.789 | 34.2189 | 225.558 | 35.6392 |
| 106.668 | 30.7939 | 162.105 | 34.3072 | 228.081 | 35.6642 |
| 107.04 | 30.8317 | 164.403 | 34.3981 | 229.114 | 35.6715 |

| | |
|---------|---------|
| 230.668 | 35.6749 |
| 233.293 | 35.6768 |
| 235.909 | 35.6804 |
| 238.515 | 35.6856 |
| 241.112 | 35.6925 |
| 243.7 | 35.7009 |
| 245.211 | 35.7036 |

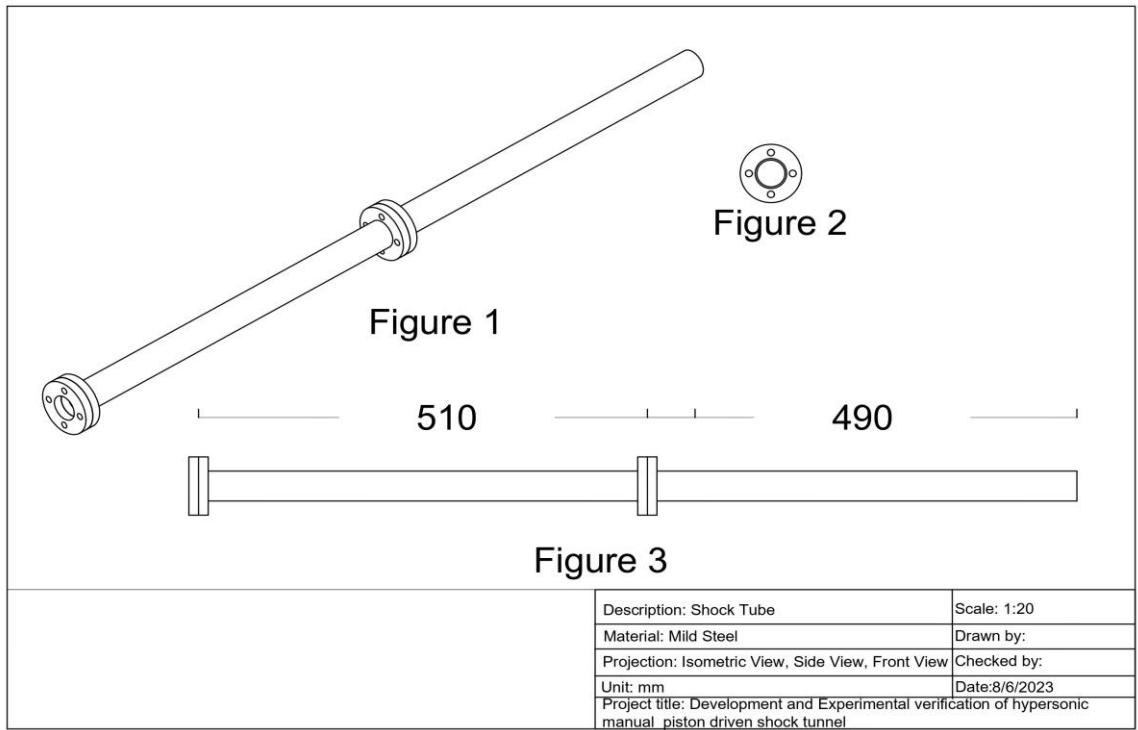
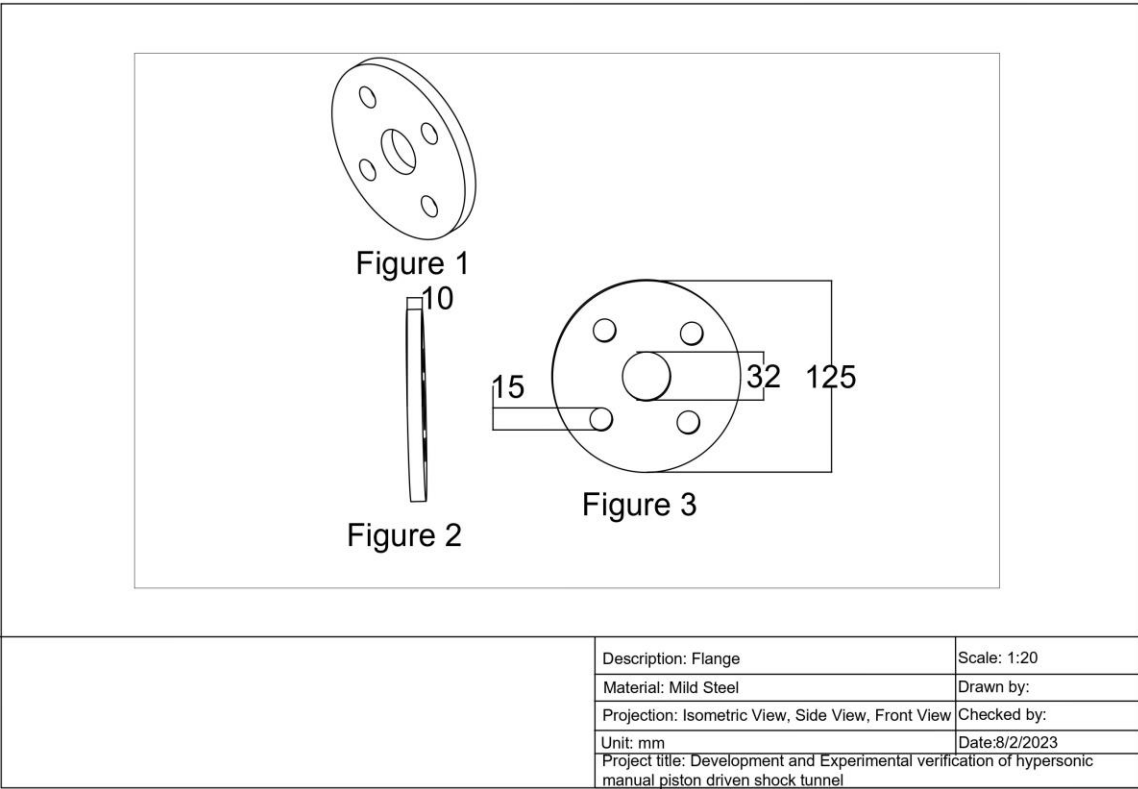
APPENDIX II

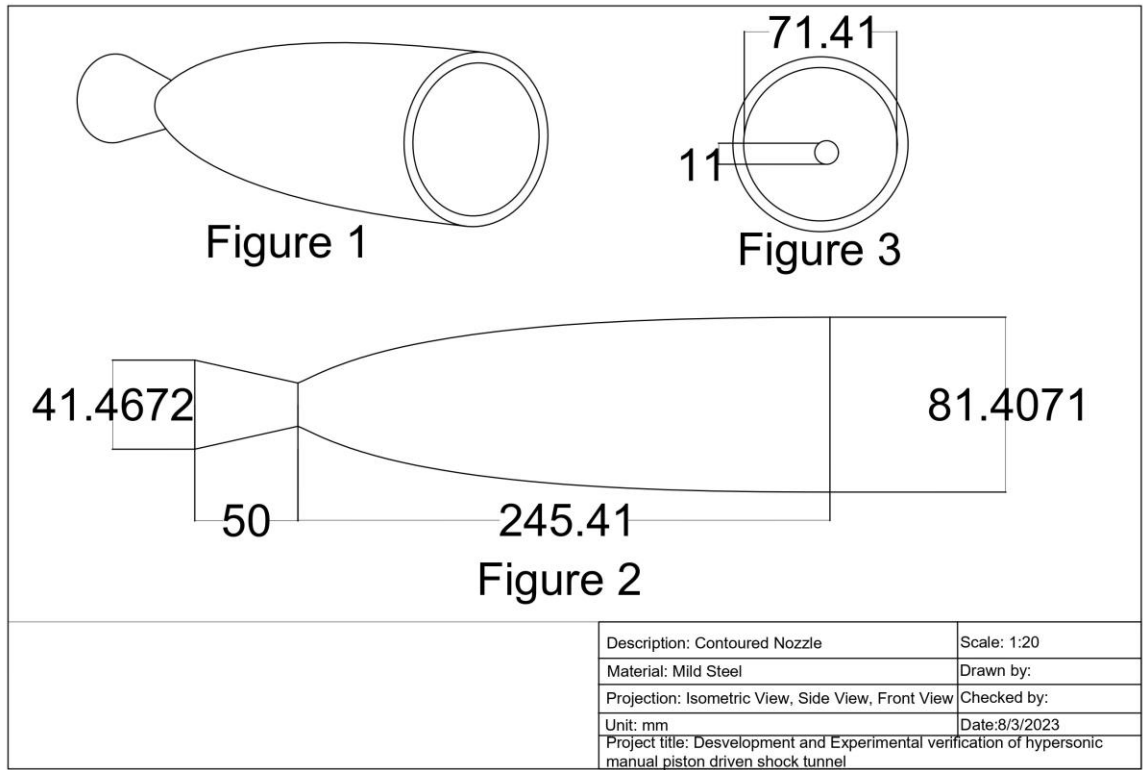
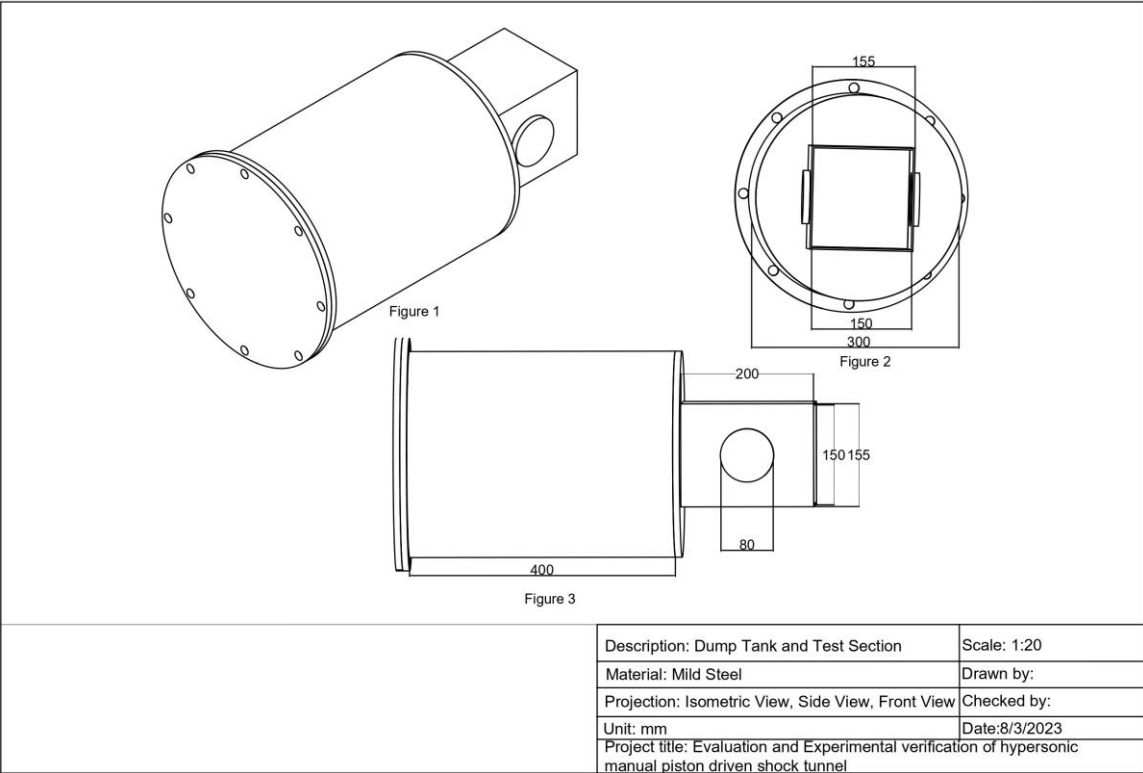












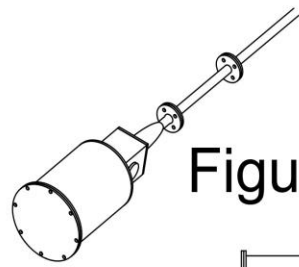


Figure 1

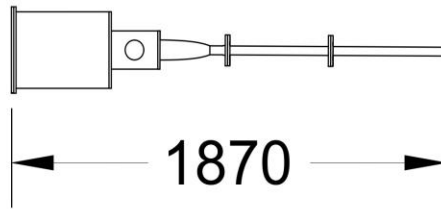


Figure 3



Figure 2

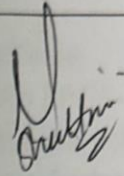
| | |
|--|----------------|
| Description: Shock tube driven hypersonic tunnel | Scale: 1:20 |
| Material: Mild Steel | Drawn by: |
| Projection: Isometric View, Side View, Top View | Checked by: |
| Unit: mm | Date: 8/3/2023 |
| Project title: Development and Experimental verification of hypersonic manual piston driven shock tunnel | |

Development and Experimental Verification of Manual Piston Driven Hypersonic Shock Tunnel

ORIGINALITY REPORT

17%

SIMILARITY INDEX



PRIMARY SOURCES

- | | | |
|---|--|----------------|
| 1 | elibrary.tucl.edu.np Internet | 305 words — 2% |
| 2 | dokumen.pub Internet | 178 words — 1% |
| 3 | "31st International Symposium on Shock Waves 2", Springer Science and Business Media LLC, 2019 Crossref | 107 words — 1% |
| 4 | 28th International Symposium on Shock Waves, 2012. Crossref | 102 words — 1% |
| 5 | Shock Waves, 2005. Crossref | 100 words — 1% |
| 6 | "30th International Symposium on Shock Waves 2", Springer Science and Business Media LLC, 2017 Crossref | 81 words — 1% |
| 7 | S.L. Gai. "Free piston shock tunnels: developments and capabilities", Progress in Aerospace Sciences, 1992 Crossref | 79 words — 1% |
| 8 | link.springer.com Internet | 72 words — 1% |

